Immunohistochemistry

The lung sections were deparaffinised and rehydrated, then microwaved in 0.01 M sodium citrate buffer for 15 min at 90°C to retrieve epitopes, and cooled at room temperature. An endogenous peroxidase blocking solution of 3% hydrogen peroxide was applied for 20 min at room temperature. After blocking the nonspecific binding sites with 2% normal goat serum, the sections were incubated with rabbit anti-mouse collagen III immunoglobulin G (IgG) (Chemicon International, Temecula, CA, USA) overnight at 4°C. The sections were then washed with PBS, followed by the addition of biotin-conjugated goat anti-rabbit IgG (Vector Laboratories Inc., Burlingame, CA, USA) and incubation for 30 min at room temperature. The sections were then washed and incubated with horseradish-peroxidase-conjugated avidin–biotin complex (Vector Laboratories Inc., Burlingame, CA, USA) at room temperature for 30 min, in accordance with the manufacturer's instructions (Vector Laboratories Inc.). The immunoreactions were visualised using 3,3′-diaminobenzidine as the substrate and counterstaining with haematoxylin.

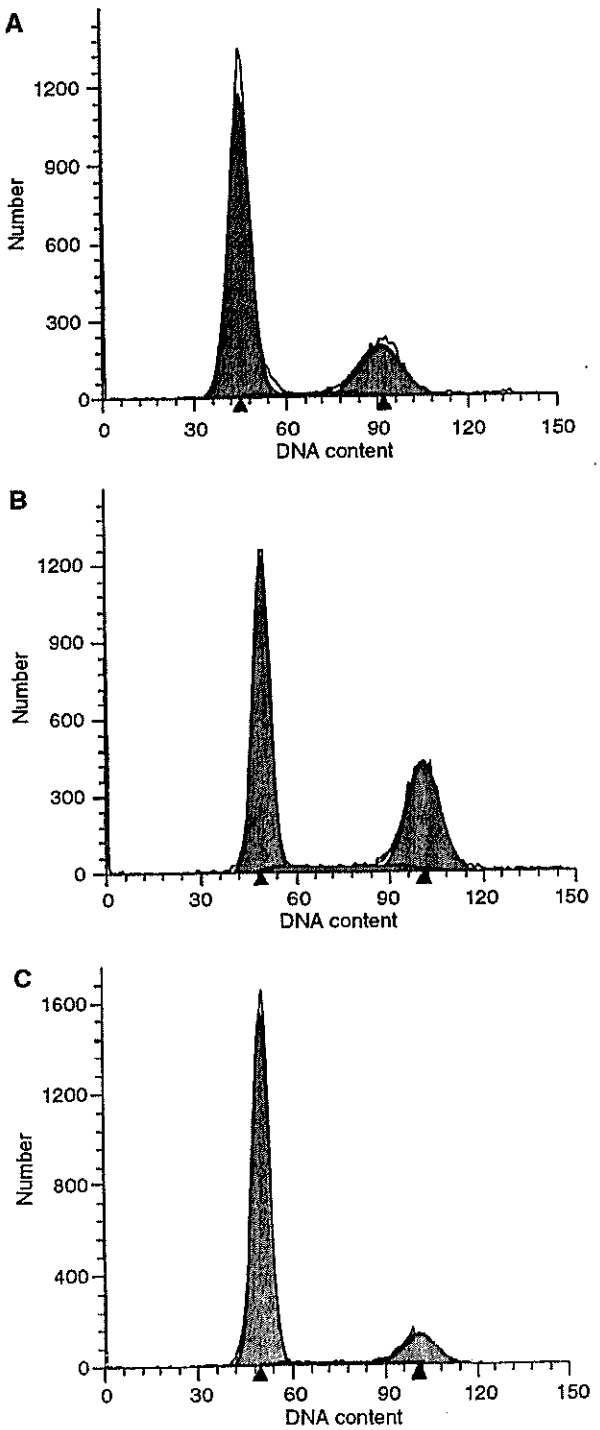

Figure 1 Cell cycle analysis. Cell cycle analysis of LLC tumour cells 24 h after PTX (**A**) or NK105 administration (**B**). Untreated control cells are shown in (**C**).

Statistical analysis

Date were expressed the mean ± s.d. Differences between the test groups were analysed by Student's *t*-test. We used Stat View (SAS Institute Inc.) statistical software. A value of $P<0.05$ was considered statistically significant.

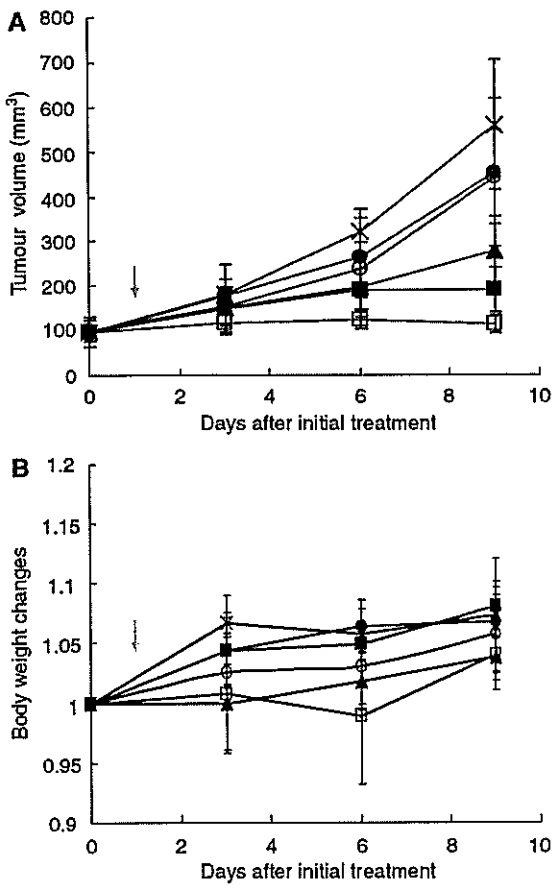

Figure 2 Antitumour activity. Changes in the LLC tumour growth rates in the mice. (**A**) Mice receiving TXL-alone (●), NK105-alone (○), combined treatment with PTX and radiation (■), and combined treatment with NK105 and radiation (□) were administered a single i.v. injection of PTX or NK105 at the dose 45 mg kg^{-1} on day 14 after the tumour inoculation (= on day 0 after the initial treatment). After 24 h the drugs were administered, the mice in the radiation-alone (△) and the combined-treatment groups were irradiated (arrow). Mice in the control group (×) were given no treatment. (**B**) Changes in the relative body weight. Data were derived from the same mice as those used in the present study.

RESULTS

Cell cycle analysis

At 24 h after the administration of PTX or NK105 to the LLC-tumour-bearing mice, severe cell cycle arrest at the G2/M phase was observed in the tumour cells treated with the drugs as compared with that in the control (no drug treatment) (Figure 1C). There was a tendency towards the NK105-treated LLC tumour cells (Figure 1B) showing more severe arrest at the G2/M phase than the PTX-treated cells (Figure 1A).

Antitumour activity

Decreased tumour growth rates of the LLC tumours were observed in the mice of the radiation alone, combined PTX with radiation, and combined NK105 with radiation groups. No antitumour activity was observed following treatment with either PTX or NK105 alone, because LLC is primarily a PTX-resistant tumour. Combined NK105 therapy with radiation yielded superior antitumour activity as compared to both radiation alone ($P=0.0047$) and combined PTX therapy with radiation ($P=0.0277$) on the day 9 after the treatment initiation (Figure 2A). No significant differences in body weight changes were noted among the groups tested (Figure 2B).

Lung toxicities

Histopathological examination of the lung sections of all the mice receiving radiation showed inflammatory cell infiltration, appearance of intra-alveolar macrophages, and destruction of the alveolar architecture. Major portions of the alveolar septa in the lung sections prepared from the irradiated mice showed slight thickening, although no massive structural destruction was observed (Figure 3A). On the other hand, the lung sections prepared from the control nonirradiated group showed no significant histopathological changes (Figure 3B). Ashcroft's fibrosis scores in the groups of mice that received radiation ranged from 0.975 to 1.426, with no significant differences among the groups. The score in the control group was nearly zero. In the groups receiving radiation, the severity of lung fibrosis differed significantly among the mice within the same groups, as did the Ashcroft's scores, that is, the s.d. of the Ashcroft's scores in the mice receiving radiation was very high (Figure 3C).

Type III collagen deposition

Immunohistochemical analysis of lung sections prepared from the mice receiving radiation revealed significant collagen deposition, especially in the subpleural regions, while that of lung sections prepared from the control group showed little collagen deposition. There were no significant differences among the different groups receiving radiation (Figure 3D).

DISCUSSION

It is well known that PTX enhances the radiosensitivity of tumour cells by inducing cell cycle arrest at the G2/M phase, the most radiosensitive phase of the cell cycle (Terasima and Tolmach, 1963;

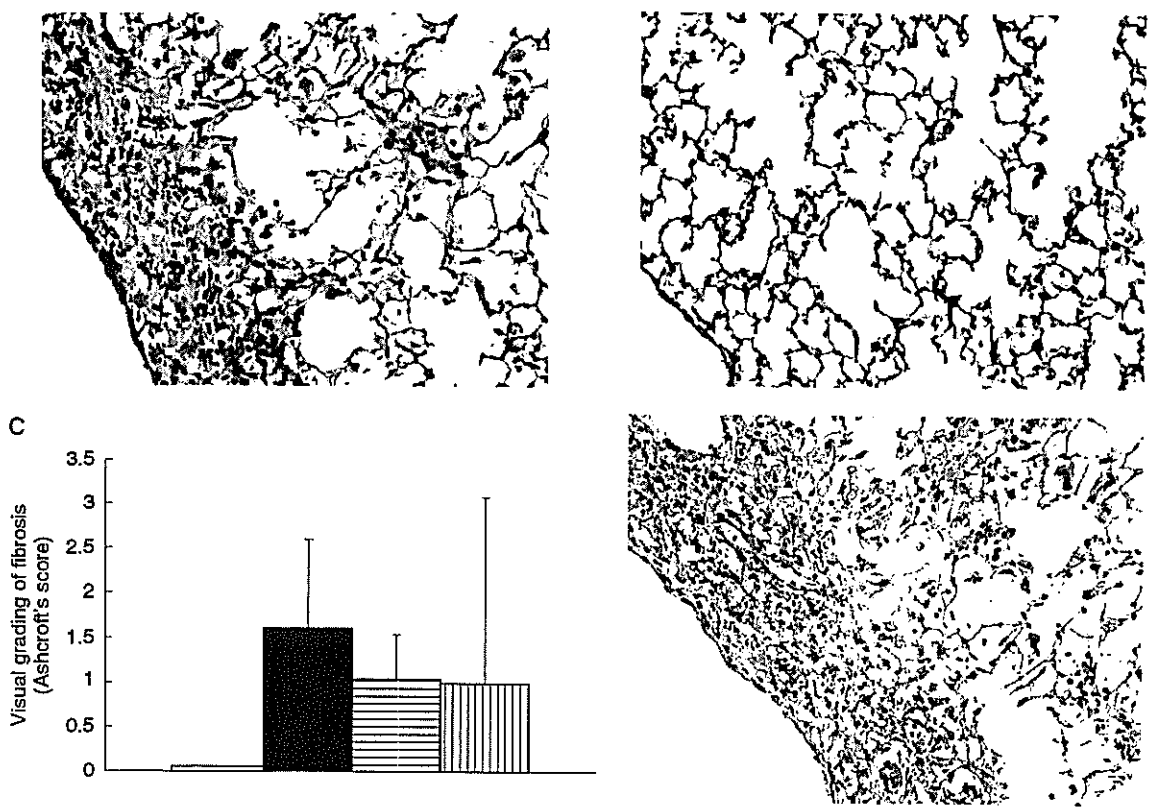

Figure 3 H&E staining of the lungs of C57BL/6J mice surviving 36 weeks after the thoracic radiation (**A**) and sham radiation (**B**). (**C**) Semiquantitative analyses to estimate the severity of pulmonary fibrosis in the mice receiving sham radiation (□), thoracic radiation alone (■), combined PTX with radiation (▤), and combined NK105 with radiation (▥). H&E- stained lung tissue sections were assessed to estimate the severity of pulmonary fibrosis by visual grading of fibrosis (Ashcroft's score). Collagen III staining of the irradiated lungs of mice (**D**).

Sinclair and Morton, 1966). Many reports have confirmed the radiosensitising effect of PTX in different cell lines (Tishler *et al*, 1992; Choy *et al*, 1993; Lokeshwar *et al*, 1995; Rodriguez *et al*, 1995), *in vivo* experiments (Milas *et al*, 1994, 1995; Cividalli *et al*, 1998), and in several clinical trials of combined PTX with radiation therapy according to different schedules (Dillman *et al*, 1990; Arriagada *et al*, 1991; Morton *et al*, 1991; Furuse *et al*, 1999; Sause *et al*, 2000; Chen *et al*, 2003). Chen *et al* (2003) examined the optimal timing of PTX treatment and irradiation in relation to the cell cycle, and recommended that radiation be given at least 5 h after PTX administration, because G2/M arrest of a lung cancer cell line was shown to start at 4 h after PTX treatment and to last for 44 h.

In our experimental model to evaluate the antitumour activity, the tumours were irradiated 24 h after a single i.v. injection of PTX or NK105. No significant increase in the antitumour activity as compared with that in the control (no treatment) was observed following a single i.v. injection of either PTX or NK105 at the dose of 45 mg kg^{-1}; LLC tumours are known to be primarily resistant to PTX. In fact, the IC_{50} of PTX against an LLC tumour cell line was shown to be 84.1 nM, which is about 10-fold higher than that of NK105 against various cancer cell lines tested in our previous work (Hamaguchi *et al*, 2005). Combined NK105 therapy with radiation yielded superior antitumour activity as compared with radiation alone or combined PTX therapy with radiation. This result suggests that NK105 has a more potent radiosensitising effect than PTX. In our study, there was a tendency towards NK105-treated LLC tumour cells showing more severe arrest at the G2/M phase as compared to PTX-treated cells at 24 h after the injection of the drugs, the timing of the radiation treatment, probably because NK105 allows a higher concentration of PTX to be maintained in the tumour than conventional PTX (Hamaguchi *et al*, 2005). We suppose that this is the reason why NK105 exerted more potent radiosensitising activity than PTX.

Next, we were concerned about the adverse effects of combined NK105 therapy with radiation. New micellar drugs are designed based on the idea that DDS can accumulate in the tumour selectively, while showing reduced distribution in normal tissues. We demonstrated that the incorporation of cisplatin into micelles significantly reduced the nephrotoxicity and neurotoxicity of cisplatin (Uchino *et al*, 2005). However, it was also shown that micelle- incorporated cisplatin caused transient liver dysfunction because it was trapped more avidly by the RES as compared to free cisplatin, even though the PEG of the outer shell of the micelle confers the so-called stealth effect.

In this study, our examination of the lung sections of mice treated with NK105 and radiation revealed that the histopathological changes such as inflammatory cell infiltration, appearance of intra-alveolar macrophages, and destruction of the alveolar architecture were induced by thoracic radiation and not by the accumulation of NK105 in the lung. There were no significant differences in the histopathological changes observed among the mice treated by NK105 and radiation and mice treated by radiation alone or PTX with radiation. The severity of lung fibrosis did not differ significantly among the test groups either. Although some clinical trials reported an increased incidence of pneumonitis and esophagitis following combined PTX therapy with radiation (Taghian *et al*, 2001; Hanna *et al*, 2002; Chen and Okunieff, 2004), others reported no influence on the incidence of such adverse effects (Ellerbroek *et al*, 2003; Yu *et al*, 2003). Several clinical trials and *in vivo* experiments have discussed the subject, however, no definitive conclusion has been arrived at (Mason *et al*, 1995; Choy *et al*, 1998; Yu *et al*, 2004; Kao *et al*, 2005). In our study, in regard to the incidence of esophagitis, there were no significant differences in the histopathological changes observed in the esophageal sections at one week after the treatment among the test groups (data not shown).

In conclusion, we demonstrated that combined NK105 chemotherapy with radiation exerts significant antitumour activity. Furthermore, the lung toxicity of this combined treatment modality was also acceptable as compared with that observed following radiation alone or combined PTX therapy with radiation. However, further studies are necessary to determine the effectiveness of NK105 in terms of its radiosensitising effect.

ACKNOWLEDGEMENTS

We thank Drs K Sugiyama and K Tsuchihara for their scientific advice and Mrs C Kanai and Mrs N Mie for their technical assistance. We are also grateful to Mrs K Shiina for her secretarial assistance. This work was supported by a Grant-in-Aid from the Ministry of Health, Labor and Welfare of Japan (Y Matsumura) and a Grant-in-Aid for Scientific Research on Priority Areas from the Ministry of Education, Culture, Sports, Science and Technology (Y Matsumura).

REFERENCES

Allen TM (1994) Long-circulating (sterically stabilized) liposomes for targeted drug delivery. *Trends Pharmacol Sci* 15: 215–220

Arriagada R, Le Chevalier T, Quoix E, Ruffie P, de Cremoux H, Douillard JY, Tarayre M, Pignon JP, Laplanche A (1991) ASTRO (American Society for Therapeutic Radiology and Oncology) plenary: Effect of chemotherapy on locally advanced non-small cell lung carcinoma: a randomized study of 353 patients. GETCB (Groupe d'Etude et Traitement des Cancers Bronchiques), FNCLCC (Federation Nationale des Centres de Lutte contre le Cancer) and the CEBI trialists. *Int J Radiat Oncol Biol Phys* 20: 1183–1190

Ashcroft T, Simpson JM, Timbrell V (1988) Simple method of estimating severity of pulmonary fibrosis on a numerical scale. *J Clin Pathol* 41: 467–470

Carney DN (1996) Chemotherapy in the management of patients with inoperable non-small cell lung cancer. *Semin Oncol* 23: 71–75

Chen Y, Okunieff P (2004) Radiation and third-generation chemotherapy. *Hematol Oncol Clin North Am* 18: 55–80

Chen Y, Pandya K, Keng PC, Johnstone D, Li J, Lee YJ, Smudzin T, Okunieff P (2003) Phase I/II clinical study of pulsed paclitaxel radiosensitization for thoracic malignancy: a therapeutic approach on the basis of preclinical research of human cancer cell lines. *Clin Cancer Res* 9: 969–975

Choy H, Akerley W, Safran H, Graziano S, Chung C, Williams T, Cole B, Kennedy T (1998a) Multiinstitutional phase II trial of paclitaxel, carboplatin, and concurrent radiation therapy for locally advanced non-small-cell lung cancer. *J Clin Oncol* 16: 3316–3322

Choy H, Devore III RF, Hande KR, Porter LL, Rosenblatt P, Yunus F, Schlabach L, Smith C, Shyr Y, Johnson DH (2000) A phase II study of paclitaxel, carboplatin, and hyperfractionated radiation therapy for locally advanced inoperable non-small-cell lung cancer (a Vanderbilt Cancer Center Affiliate Network Study). *Int J Radiat Oncol Biol Phys* 47: 931–937

Choy H, Rodriguez FF, Koester S, Hilsenbeck S, Von Hoff DD (1993) Investigation of taxol as a potential radiation sensitizer. *Cancer* 71: 3774–3778

Choy H, Safran H, Akerley W, Graziano SL, Bogart JA, Cole BF (1998b) Phase II trial of weekly paclitaxel and concurrent radiation therapy for locally advanced non-small cell lung cancer. *Clin Cancer Res* 4: 1931–1936

Cividalli A, Arcangeli G, Cruciani G, Livdi E, Cordelli E, Danesi DT (1998) Enhancement of radiation response by paclitaxel in mice according to different treatment schedules. *Int J Radiat Oncol Biol Phys* 40: 1163–1170

Dillman RO, Seagren SL, Propert KJ, Guerra J, Eaton WL, Perry MC, Carey RW, Frei III EF, Green MR (1990) A randomized trial of induction

chemotherapy plus high-dose radiation *vs* radiation alone in stage III non-small-cell lung cancer. *N Engl J Med* 323: 940–945

Dowell JE, Sinard R, Yardley DA, Aviles V, Machtay M, Weber RS, Weinstein GS, Chalian AA, Carbone DP, Rosenthal DI (1999) Seven-week continuous-infusion paclitaxel concurrent with radiation therapy for locally advanced non-small cell lung and head and neck cancers. *Semin Radiat Oncol* 9: 97–101

Early Breast Cancer Trialists' Collaborative Group (2000) Favourable and unfavourable effects on long-term survival of radiotherapy for early breast cancer: an overview of the randomised trials. Early Breast Cancer Trialists' Collaborative Group. *Lancet* 355: 1757–1770

Ellerbroek N, Martino S, Mautner B, Tao ML, Rose C, Botnick L (2003) Breast-conserving therapy with adjuvant paclitaxel and radiation therapy: feasibility of concurrent treatment. *Breast J* 9: 74–78

Formenti SC, Volm M, Skinner KA, Spicer D, Cohen D, Perez E, Bettini AC, Groshen S, Gee C, Florentine B, Press M, Danenberg P, Muggia F (2003) Preoperative twice-weekly paclitaxel with concurrent radiation therapy followed by surgery and postoperative doxorubicin-based chemotherapy in locally advanced breast cancer: a phase I/II trial. *J Clin Oncol* 21: 864–870

Furuse K, Fukuoka M, Kawahara M, Nishikawa H, Takada Y, Kudoh S, Katagami N, Ariyoshi Y (1999) Phase III study of concurrent *vs* sequential thoracic radiotherapy in combination with mitomycin, vindesine, and cisplatin in unresectable stage III non-small-cell lung cancer. *J Clin Oncol* 17: 2692–2699

Gabizon A, Chemla M, Tzemach D, Horowitz AT, Goren D (1996) Liposome longevity and stability in circulation: effects on the *in vivo* delivery to tumors and therapeutic efficacy of encapsulated anthracyclines. *J Drug Target* 3: 391–398

Hamaguchi T, Matsumura Y, Suzuki M, Shimizu K, Goda R, Nakamura I, Nakatomi I, Yokoyama M, Kataoka K, Kakizoe T (2005) NK105, a paclitaxel-incorporating micellar nanoparticle formulation, can extend *in vivo* antitumour activity and reduce the neurotoxicity of paclitaxel. *Br J Cancer* 92: 1240–1246

Hanna YM, Baglan KL, Stromberg JS, Vicini FA, A Decker D (2002) Acute and subacute toxicity associated with concurrent adjuvant radiation therapy and paclitaxel in primary breast cancer therapy. *Breast J* 8: 149–153

Kao J, Conzen SD, Jaskowiak NT, Song DH, Recant W, Singh R, Masters GA, Fleming GF, Heimann R (2005) Concomitant radiation therapy and paclitaxel for unresectable locally advanced breast cancer: results from two consecutive phase I/II trials. *Int J Radiat Oncol Biol Phys* 61: 1045–1053

Khayat D, Antoine EC, Coeffic D (2000) Taxol in the management of cancers of the breast and the ovary. *Cancer Invest* 18: 242–260

Klibanov AL, Maruyama K, Beckerleg AM, Torchilin VP, Huang L (1991) Activity of amphipathic poly(ethylene glycol) 5000 to prolong the circulation time of liposomes depends on the liposome size and is unfavorable for immunoliposome binding to target. *Biochim Biophys Acta* 1062: 142–148

Klibanov AL, Maruyama K, Torchilin VP, Huang L (1990) Amphipathic polyethyleneglycols effectively prolong the circulation time of liposomes. *FEBS Lett* 268: 235–237

Lind PA, Marks LB, Hardenbergh PH, Clough R, Fan M, Hollis D, Hernando ML, Lucas D, Piepgrass A, Prosnitz LR (2002) Technical factors associated with radiation pneumonitis after local +/− regional radiation therapy for breast cancer. *Int J Radiat Oncol Biol Phys* 52: 137–143

Lokeshwar BL, Ferrell SM, Block NL (1995) Enhancement of radiation response of prostatic carcinoma by taxol: therapeutic potential for late-stage malignancy. *Anticancer Res* 15: 93–98

Maeda H, Matsumura Y (1989) Tumoritropic and lymphotropic principles of macromolecular drugs. *Crit Rev Ther Drug Carrier Syst* 6: 193–210

Mason KA, Milas L, Peters LJ (1995) Effect of paclitaxel (taxol) alone and in combination with radiation on the gastrointestinal mucosa. *Int J Radiat Oncol Biol Phys* 32: 1381–1389

Matsumura Y, Maeda H (1986) A new concept for macromolecular therapeutics in cancer chemotherapy: mechanism of tumoritropic accumulation of proteins and the antitumor agent smancs. *Cancer Res* 46: 6387–6392

Milas L, Hunter NR, Mason KA, Kurdoglu B, Peters LJ (1994) Enhancement of tumour radioresponse of a murine mammary carcinoma by paclitaxel. *Cancer Res* 54: 3506–3510

Milas L, Hunter NR, Mason KA, Milross CG, Saito Y, Peters LJ (1995) Role of reoxygenation in induction of enhancement of tumour radioresponse by paclitaxel. *Cancer Res* 55: 3564–3568

Morton RF, Jett JR, McGinnis WL, Earle JD, Therneau TM, Krook JE, Elliott TE, Mailliard JA, Nelimark RA, Maksymiuk AW (1991) Thoracic radiation therapy alone compared with combined chemoradiotherapy for locally unresectable non-small cell lung cancer. A randomized, phase III trial. *Ann Intern Med* 115: 681–686

Penney DP, Rubin P (1977) Specific early fine structural changes in the lung irradiation. *Int J Radiat Oncol Biol Phys* 2: 1123–1132

Rodriguez M, Sevin BU, Perras J, Nguyen HN, Pham C, Steren AJ, Koechli OR, Averette HE (1995) Paclitaxel: a radiation sensitizer of human cervical cancer cells. *Gynecol Oncol* 57: 165–169

Rowinsky EK, Chaudhry V, Forastiere AA, Sartorius SE, Ettinger DS, Grochow LB, Lubejko BG, Cornblath DR, Donehower RC (1993) Phase I and pharmacologic study of paclitaxel and cisplatin with granulocyte colony-stimulating factor: neuromuscular toxicity is dose-limiting. *J Clin Oncol* 11: 2010–2020

Rowinsky EK, Donehower RC (1995) Paclitaxel (taxol). *N Engl J Med* 332: 1004–1014

Sause W, Kolesar P, Taylor SI, Johnson D, Livingston R, Komaki R, Emami B, Curran Jr W, Byhardt R, Dar AR, Turrisi III A (2000) Final results of phase III trial in regionally advanced unresectable non-small cell lung cancer: Radiation Therapy Oncology Group, Eastern Cooperative Oncology Group, and Southwest Oncology Group. *Chest* 117: 358–364

Sinclair WK, Morton RA (1966) X-ray sensitivity during the cell generation cycle of cultured Chinese hamster cells. *Radiat Res* 29: 450–474

Taghian AG, Assaad SI, Niemierko A, Kuter I, Younger J, Schoenthaler R, Roche M, Powell SN (2001) Risk of pneumonitis in breast cancer patients treated with radiation therapy and combination chemotherapy with paclitaxel. *J Natl Cancer Inst* 93: 1806–1811

Terasima T, Tolmach LJ (1963) X-ray sensitivity and DNA synthesis in synchronous populations of HeLa cells. *Science* 140: 490–492

Tishler RB, Geard CR, Hall EJ, Schiff PB (1992) Taxol sensitizes human astrocytoma cells to radiation. *Cancer Res* 52: 3495–3497

Uchino H, Matsumura Y, Negishi T, Koizumi F, Hayashi T, Honda T, Nishiyama N, Kataoka K, Naito S, Kakizoe T (2005) Cisplatin-incorporating polymeric micelles (NC-6004) can reduce nephrotoxicity and neurotoxicity of cisplatin in rats. *Br J Cancer* 93: 678–687

Weiss RB, Donehower RC, Wiernik PH, Ohnuma T, Gralla RJ, Trump DL, Baker Jr JR, Van Echo DA, Von Hoff DD, Leyland-Jones B (1990) Hypersensitivity reactions from taxol. *J Clin Oncol* 8: 1263–1268

Yu TK, Whitman GJ, Thames HD, Strom E, McNeese MD, Perkins GH, Schechter N, Kau S, Buzdar AU, Hortobagyi GN, Thomas E, Buchholz TA (2003) Clinically-relevant pneumonitis is not increased in breast cancer patients treated with sequential paclitaxel and radiation. *Int J Radiat Oncol Biol Phys* 57(2 Suppl): S127–S128

Yu TK, Whitman GJ, Thames HD, Buzdar AU, Strom EA, Perkins GH, Schechter NR, McNeese MD, Kau SW, Thomas ES, Hortobagyi GN, Buchholz TA (2004) Clinically relevant pneumonitis after sequential paclitaxel-based chemotherapy and radiotherapy in breast cancer patients. *J Natl Cancer Inst* 96: 1676–1681

Lung Cancer (2006) 53, 13–21

available at www.sciencedirect.com

SCIENCE DIRECT®

journal homepage: www.elsevier.com/locate/lungcan

Effects of different combinations of gefitinib and irinotecan in lung cancer cell lines expressing wild or deletional EGFR

Tatsu Shimoyama[a,b], Fumiaki Koizumi[a], Hisao Fukumoto[a], Katsuyuki Kiura[b], Mitsune Tanimoto[b], Nagahiro Saijo[a], Kazuto Nishio[a,*]

[a] *Shien-Lab and Medical Oncology, National Cancer Center Hospital, Pharmacology Division, National Cancer Center Research Institute, Tsukiji 5-1-1, Chuo-ku, Tokyo 104-0045, Japan*
[b] *Department of Medicine II, Okayama University Medical School, 2-5-1 Shikata-cho, Okayama 700-8558, Japan*

Received 8 November 2005; accepted 1 March 2006

KEYWORDS
Gefitinib;
CPT-11;
SN-38;
EGFR;
Combination;
Lung cancer

Summary EGFR mutations are a major determinant of lung tumor response to gefitinib, an EGFR-specific tyrosine kinase inhibitor. Obtaining a response from lung tumors expressing wild-type EGFR is a major obstacle. The combination of gefitinib and cytotoxic drugs is one strategy against lung cancers expressing wild-type EGFR. The DNA topoisomerase inhibitor irinotecan sulfate (CPT-11) is active against lung cancer. We examined the sensitivity of lung cancers expressing wild- or mutant-type EGFR to the combination of gefitinib and CPT-11. The in vitro effect of gefitinib and SN-38 (the active metabolite of CPT-11) was examined in seven lung cancer cell lines using the dye formation assay with a combination index. When administered concurrently, gefitinib and SN-38 had a synergistic effect in five of the seven cell lines expressing wild-type EGFR, whereas the combination was antagonistic in PC-9 cells and a PC-9 subline resistant to gefitinib and expressing deletional mutant EGFR (PC-9/ZD). When administered sequentially, treatment with SN-38 followed by gefitinib had remarkable synergistic effects in the PC-9 and PC-9/ZD cells. In an in vivo tumor-bearing model, this combination had a schedule-dependent synergistic effect in the PC-9 and PC-9/ZD cells. An immunohistochemical analysis of the tumors in mice treated with CPT-11 and gefitinib demonstrated that the number of Ki-67 positive tumor cells induced by CPT-11 treatment was decreased when CPT-11 was administered in combination with gefitinib. In conclusion, the sequential combination of CPT-11 and gefitinib is considered to be active against lung cancer.

1. Introduction

Lung cancer is one of the leading causes of cancer-related death, despite the use of conventional chemotherapy regi-

* Corresponding author at: Tel.: +81 3 3542 2511; fax: +81 3 3547 5185.
E-mail address: knishio@gan2.res.ncc.go.jp (K. Nishio).

0169-5002/$ – see front matter © 2006 Elsevier Ireland Ltd. All rights reserved.
doi:10.1016/j.lungcan.2006.03.014

mens. The epidermal growth factor receptor (EGFR) is frequently expressed in non-small cell lung cancer (NSCLC) and is correlated with a poor prognosis. Gefitinib ('Iressa') is an orally active, selective EGFR-tyrosine kinase inhibitor that blocks signal transduction pathways. Its clinical efficacy has been show in refractory NCSLC patients, but the survival benefit of this agent remains unclear. EGFR mutations have been identified in NSCLC, and lung cancers carrying the EGFR mutation have been reported to be hyperresponsive to gefitinib [1,2]. Mutant EGFR is a major determinant of lung tumor response to gefitinib, but the hyperresponsiveness of tumors expressing mutant EGFR has been observed in a small population. Now, obtaining a clinical benefit in lung tumors expressing wild-ype EGFR is a major obstacle. The combination of gefitinib and cytotoxic drugs is one strategy against lung cancers expressing wild-type EGFR. The DNA topoisomerase I inhibitor irinotecan (CPT-11) is a key drug in the treatment of patients with lung cancer and has been shown to prolong survival. SN-38 is the active metabolite of CPT-11 in vitro. The objective of this study was to determine the potential therapeutic utility of gefitinib when combined with CPT-11 therapy to lung cancer cell according to the treatment schedule and EGFR status.

Acquired resistance to gefitinib is also of clinical interest. Recently, Kobayashi et al. [3] reported that an EGFR mutation was related to the development of acquired resistance to gefitinib. We have established subclone PC-9/ZD cells that are resistant to gefitinib [4]. Our results suggested that another mechanism of resistance was active in PC-9/ZD cells. The effect of the combination of gefitinib and SN-38 in these PC-9/ZD cells was also examined.

2. Materials and methods

2.1. Drugs and chemicals

Gefitinib (*N*-(3-chloro-4-fluorophenyl)-7-methoxy-6-[3-(morpholin-4-yl)propoxy]quinazolin-4-amine) was provided by AstraZeneca (Cheshire, UK). Gefitinib was dissolved in dimethyl sulfoxide (DMSO) for the in vitro study. CPT-11 and SN-38 were obtained from Yakult Honsha (Tokyo, Japan) and were dissolved in dimethyl sulfoxide (DMSO) for both of the in vitro studies.

2.2. Cells and cultures

Human NSCLC cell lines PC-9, PC-7, and PC-14 derived from untreated patients with pulmonary adenocarcinoma were provided by Professor Y. Hayata, Tokyo Medical College. A small cell lung cancer cell line, H69, was established at the National Cancer Institute (Bethesda, MD, USA). The gefitinib-resistant subline, PC-9/ZD, was established from intrinsic hypersensitive cell PC-9 [5] in our laboratory [4]. A small cell lung cancer cell line, SBC-3, and an adenocarcinoma cell line, A549, were obtained from the Japanese Cancer Research Resources Bank (Tokyo, Japan). All cell lines were maintained in RPMI1640 (Nikken Bio Med. Lab., Kyoto, Japan) supplemented with 10% heat-inactivated fetal calf serum, 100 μg/ml streptomycin, and 100 units/ml penicillin in an incubator at 37 °C and 100% humidity in 5% CO_2 and air, as described previously [6].

2.3. RT-PCR

Specific primers designed for EGFR CDS were used to detect the EGFR mRNA, as described elsewhere [1]. Sixteen first-strand cDNAs were synthesized from the cells' RNA using an RNA PCR Kit (TaKaRa Biomedicals, Ohtsu, Japan). After the reverse transcription of 1 μg of total RNA with Oligo(dT)-M4 adaptor primer, the whole mixture was used for PCR with two oligonucleotide primers (5′-AATGTGAGCAGAGGCAGGGA-3′ and 5′-GGCTTGGTTTGGAGCTTCTC-3). PCR was performed with an initial denaturation at 94 °C for 2 min and 25 cycles of amplification (denaturation at 94 °C for 30 s, annealing at 55 °C for 60 s, and extension at 72 °C for 105 s).

2.4. Western blot analysis

The cultured cells were washed twice with ice-cold phosphate buffered saline (PBS), lysate in EBC buffer (50 mM Tris–HCl, pH 8.0; 120 mM NaCl; 0.5% Nonidet P-40; 100 mM NaF; 200 mM Na orthovanadate; and 10 mg/ml each of leupeptin, aprotinin and phenylmethylsulfonyl fluoride). The lysate was cleared by centrifugation at 20,000 × *g* for 5 min, and the protein concentration of the supernatant was measured using a BCA protein assay (Pierce, Rockford, IL, USA). For immunoblotting, 20 μg samples of protein were electrophoretically separated on a 7.5% SDS-polyacrylamide gel and transferred to a polyvinylidene difluoride (PVDF) membrane (Millipore, Bedford, MA, USA). The membrane was then probed with rabbit polyclonal antibodies against EGFR, HER2/neu, Her3 and Her4 (Santa Cruz Biotech, Santa Cruz, CA, USA) and phospho-EGFR specific for Tyr 845, Tyr 1045, and Tyr 1068 (numbers 2231, 2235 and 2234; Cell Signaling, Beverly, MA, USA).

2.5. Growth-inhibition assay

We used the tetrazolium dye (3,(4,5-dimethyl-2-thiazolyl)-2,5-diphenyl-2H-tetrazolium bromide, MTT) assay to evaluate the cytotoxicity of various drug concentrations. After incubation for 72 h at 37 °C, 20 μl of MTT solution (5 mg/ml in PBS) was added to each well; the plates were then incubated for a further 4 h at 37 °C. After centrifuging the plates at 200 × *g* for 5 min, the medium was aspirated from each well and 180 μl of dimethylsulfoxide was added to each well to dissolve the formazan. Optical density was measured at 562 and 630 nm using a Delta Soft ELISA analysis program interfaced with a Bio-Tek Microplate Reader (EL-340; Bio-Metallics, Princeton, NJ, USA). Each experiment was performed in six replicate wells for each drug concentration and was independently performed three or four times. The IC_{50} value was defined as the concentration needed for a 50% reduction in the absorbance, as calculated based on the survival curves. Percent survival was calculated as follows:

$$\frac{\text{Mean absorbance of six replicate wells containing drugs} - \text{mean absorbance of six replicate background wells}}{\text{mean absorbance of six replicate drug-free wells} - \text{mean absorbance of six replicate background wells}} \times 100.$$

2.6. Combined effect of gefitinib and SN-38 in vitro

After 24 h of incubation, gefitinib and SN-38 were added to each cell line according to one of the two combination schedules. For the concurrent schedule, gefitinib and SN-38 were added concurrently and were then incubated under the same conditions for 72 h. For the sequential schedule, gefitinib or SN-38 were added sequentially and were then incubated under the same conditions for 72 h. The combined effect of gefitinib and SN-38 on lung cancer cell growth was evaluated using a combination index (CI) [7]. The CI was produced using CalcuSym software (Biosoft, NY, USA). For any given drug combination, the CI represents the degree of synergy, additivity, or antagonism. CI was expressed in terms of fraction-affected (F_a) values, which represents the percentage of cells killed or inhibited by the drug. Using mutually exclusive ($\alpha = 0$) or mutually non-exclusive ($\alpha = 1$) isobologram equations, the F_a/CI plots for each cell line were constructed by computer analysis of the data generated from the median effect analysis. The CI values were interpreted as follows: <1.0 = synergism; 1.0 = additive; >1.0 = antagonism.

2.7. In vivo growth-inhibition assay

Experiments were performed in accordance with the United Kingdom Coordinating Committee on Cancer Research Guidelines for the welfare of animals with experimental neoplasia (second edition). Fig. 2A shows the treatment schedule. For the in vivo experiments, the combined therapeutic effect of orally or intraperitoneally administered gefitinib and intravenously injected CPT-11 was evaluated according to a predetermined schedule. The dose of each drug was set based on the results of a preliminary experiment involving the administration of each drug alone. Ten days before administration, PC-9 and PC-9/ZD cells were injected subcutaneously into the backs of the mice. Six mice per group were injected with tumor cells. Tumor-bearing mice were given either gefitinib (40 mg/kg/day, p.o.) on days 2–6, CPT-11 (50 mg/kg/day, i.v.) on day 1, both, or a placebo (5%(w/v) glucose solution). Alternatively, tumor-bearing mice were given gefitinib on days 2–6 and CPT-1 on days 2. The diameters of the tumors were measured using calipers on days 1, 5, 8, 12, 15 and 20 to evaluate the effects of treatment, and tumor volume was determined using the following equation: tumor volume $ab^2/2$ (mm^3) (where a is the largest diameter of the tumor and b is the shortest diameter). Day 20 denotes the day on which the effects of the drugs were estimated, and day "0" denotes the first day of treatment. All mice were sacrificed on day 20 after their tumors had been measured.

2.8. Immunohistochemistry

The tumors were harvested from the mice at the time of sacrifice. For hematoxylin-eosin (HE) and anti-CD31 and Ki-67 staining, the resected tumors were fixed in zinc-buffered formalin (Shandon Lipshaw, Pittsburgh, PA) overnight at 4 °C. After paraffin embedding and sectioning at 6 μm, formalin-fixed sections were stained with Mayer's H&E (Richard Allen, Kalamazoo, MI, USA). For anti-Ki-67 and anti-CD31 immunohistochemistry, the slides were heated in a water bath at 95–99 °C in Target Retrieval Solution (DAKO, Carpinteria, CA, USA) for 20 min, followed by a 20-min cool-down period at room temperature. After heat retrieval, the sections were rinsed well in PBS and stained with rabbit antihuman Ki-67 antigen (DAKO N-series, ready to use) or rat antimouse CD-31 antibody (BD PharMingen, Tokyo, Japan) according to the manufacturer's instructions and then were lightly counterstained with Mayer's hematoxylin. The sections were finally stained with an in situ Death Detection POD Kit (Roche Diagnostic GmbH, Mannheim, Germany), according to the manufacturer's instructions.

TUNEL staining was performed using the Apoptosis Detection System, Fluorescein (Promega, Madison, WI, USA). Briefly, 6-μm cryostat sections were fixed in 4% paraformaldehyde for 10 min at room temperature and rinsed in PBS with 0.1% Triton X-100. The sections were then incubated in Equilibration Buffer for 5 min at room temperature followed by incubation in TUNEL Mix, prepared according to the manufacturer's instructions, for 1 h at 37 °C. After successive washes in PBS, the sections were coverslipped using an antifade reagent.

Microvessel density was determined by calculating the proportion of CD31-positive cells. The Proliferation Index was determined by Ki-67 immunostaining and calculating the population of Ki-67-positive cells in five fields at 200×. The Apoptosis Index, determined by TUNEL staining, was calculated from the population of TUNEL-positive cells in five fields at 200×. The apoptosis:proliferation ratio equals the apoptosis index/proliferation index × 100. At least 1000 tumor cell nuclei from the most evenly and distinctly labeled areas were examined in each examination.

At least 1000 cancer cells were counted and scored per slide. Both the percentage of specifically stained cells and the intensity of immunostaining were recorded. Blood vessels were detected with an anti-von Willebrand factor (vWF) antibody (Chemicon). Microvessel density was determined by calculating the proportion of vWF-positive cells.

3. Results

3.1. Expression of Her-receptors and cellular sensitivity to gefitinib or SN-38 in lung cancer cell lines

The expression levels of EGFR in seven lung cancer cell lines were examined using RT-PCR with a primer set for exon 20 in EGFR. PC-14, SBC-3, H69, PC-7, and A549 cells showed a 570-bp-long PCR amplified product exhibiting wild-type EGFR mRNA (data not shown). On the other hand, a smaller PCR product was also detected in the PC-9 and PC-9/ZD cells, and this band was confirmed to be an in-frame 15-base deletion of exon 20 (E746_A750del).

We examined the protein levels of EGFR, Her2, Her3, and Her4 in the lung cell lines using immunoblotting. The quantitative data obtained by densitometorical analysis is summarized in Table 1. The protein levels of EGFR, Her2, and Her3 in the PC-9 cells were one- to four-fold higher than those in the other cell lines (PC-7, H69, PC-14, A549, and SBC-3).

Table 1 Comparison of Her family protein levels and gefitinib- and SN-38-induced growth inhibition

Cell lines	Relative expression[a]				Growth inhibition[b], $IC_{50} \pm$ S.D.	
	EGFR	Her2	Her3	Her4	Gefitinib (μM)	SN-38 (nM)
PC-9	2.8[c]	3.2	3.7	ND	0.047 ± 0.061	8.09 ± 1.9
PC-9/ZD	1.6[c]	2.6	3.8	ND	7.7 ± 0.5	38.9 ± 7.0
PC-14	1.5	2.8	1.1	ND	17.1 ± 0.8	42.1 ± 2.6
SBC-3	2.4	2.6	1.0	ND	19.9 ± 5.4	1.07 ± 0.1
A549	2.3	2.3	1.4	ND	30.2 ± 2.2	293 ± 64.5
H69	1.3	1.3	2.0	ND	56.5 ± 3.2	27.2 ± 4.1
PC-7	1.0	1.0	1.2	ND	68.8 ± 14.8	20.5 ± 8.2

The IC_{50} value (μM) of each drug was measured by MTT assay, as described in Section 2. Each value is the mean ± S.D. of three or four independent experiments.

[a] Protein expression levels were analyzed by Western blotting.

[b] Drug concentration responsible for 50% growth inhibition in MTT assay at 72 h, calculated data for at least three dependent experiments.

[c] 15-base deletion EGFR, ND: not determined.

3.2. Cellular sensitivity of lung cancer cells to gefitinib and SN-38

The growth inhibitory effect of gefitinib and SN-38 on lung cancer cells was examined using an MTT assay. The IC_{50} values of gefitinib for the cell lines ranged from 46 nM (PC-9 cells) to 68 μM (PC-7 cells). The PC-9/ZD cells were ~200-fold resistant to gefitinib, compared with the parental PC-9 cells. Cellular sensitivity to gefitinib and the expression levels of EGFR and Her2 were negatively correlated with the IC_{50} values of gefitinib (Table 1). The IC_{50} values of SN-38 for these cell lines ranged from 1 nM (SBC-3) to 300 nM (A549). The range of sensitivity to gefitinib was wider than that to SN-38. No correlation in cellular sensitivity to gefitinib and SN-38 was seen.

3.3. In vitro combined effect of gefitinib and SN-38 on lung cancer cell lines

To evaluate the potential combined effect of gefitinib and SN-38, the combination index was determined using an MTT assay. The combined effects of gefitinib and SN-38 under the concurrent schedule are shown in Fig. 1. CI values of <1, >1, and 1 indicate a supra-additive effect (synergism), an antagonistic effect, and an additive effect, respectively. An additive to supra-additive growth-inhibitory effect was observed for all doses of gefitinib and SN-38 tested in cell lines expressing wild-type EGFR. On the other hand, a high CI index was observed in PC-9 cells and PC-9/ZD cells expressing mutant EGFR over a wide range of inhibition levels. These results suggest that gefitinib and SN-38 are synergistic in lung cancer cells expressing wild-type EGFR but not in cell lines expressing mutant EGFR in vitro.

3.4. Schedule-dependent synergy of gefitinib and SN-38 in lung cancer cells

Next, we examined the schedule dependency of the combined effects of gefitinib and SN-38 in the cell lines. The five cell lines expressing wild-type EGFR showed synergistic (PC-14, H69, and A549 cells) or additive effects (SBC-3 and PC-7 cells) for all three schedules: concurrent administration, SN-38 followed by gefitinib administration, and gefitinib followed by SN-38 administration (Fig. 1A). In the PC-9 cells, concurrent administration and gefitinib followed by SN-38 administration were antagonistic, but SN-38 followed by gefitinib administration was synergistic (Fig. 1B). In the PC-9/ZD cells, concurrent administration was antagonistic, but sequential administration was synergistic. These schedule-dependent combined effects were observed in the cells expressing mutant EGFR.

3.5. Combined effects of gefitinib and SN-38 in vivo

To estimate the schedule-dependent effects in vivo, nude mice bearing tumors were treated with gefitinib and CPT-11 according to sequential or concurrent schedules (Fig. 2A). Mice bearing PC-14 tumors were treated with gefitinib and CPT-11 according to sequential or concurrent schedules. CPT-11 (50 mg/kg) alone potentially reduced the tumor size, and the combination of gefitinib and CPT-11 was synergistic. In particular, the administration of CPT-11 followed by gefitinib cured the mice bearing PC-14 cells (Fig. 2B).

Mice bearing PC-9 or PC-9/ZD tumors were treated with gefitinib and CPT-11 according to sequential or concurrent schedules. Gefitinib (40 mg/kg) alone potentially reduced the PC-9 tumors, and CPT-11 (50 mg/kg) followed by gefitinib administration reduced the tumor size of PC-9 xenografts more dramatically (gefitinib alone: $P=0.012$, sequential combination: $P=0.005$) (Fig. 2B). On the other hand, the concurrent schedule produced an antagonistic effect. Body weight loss was not observed in any of the mice treated according to the above schedules (Fig. 2C). CPT-11 followed by gefitinib administration is a potentially beneficial schedule against PC-9 and PC-9/ZD cells expressing mutational EGFR. The results of these in vivo experiments were consistent with those of the in vitro studies.

To elucidate the synergistic mechanisms of CPT-11 and gefitinib in vivo, tumor samples of the PC-9 and PC-9/ZD

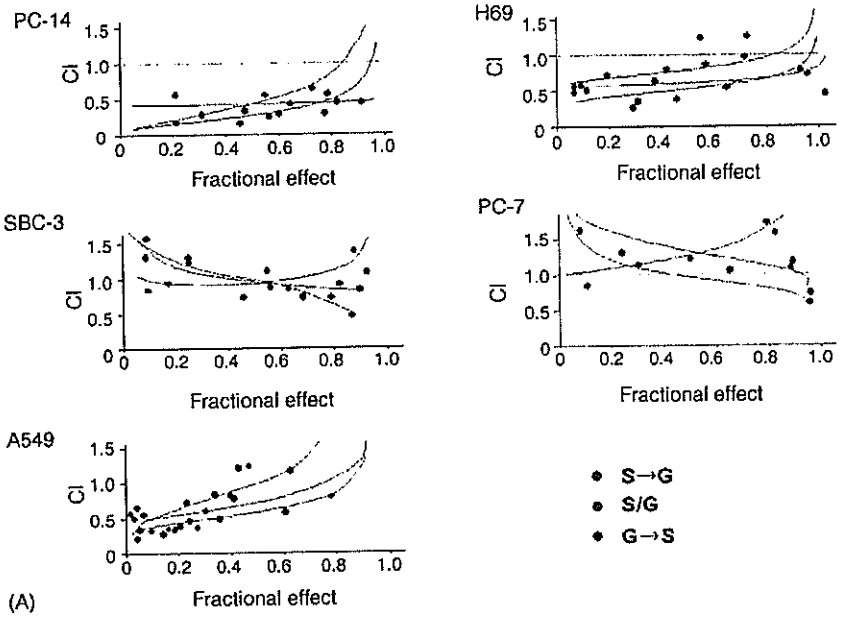

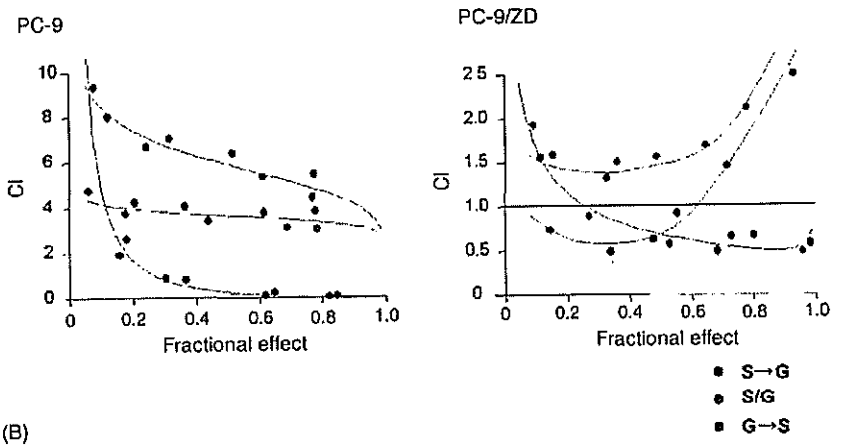

Fig. 1 Combination index (CI) plots of interactions between gefitinib and SN-38 in lung cancer cell lines. Each cell line was treated with gefitinib and SN-38, either alone or in combination at a fixed molar ratio. (A) (PC-14) gefitinib: SN-38 = 425:1; (SBC-3) 20000:1; (A549) 100:1; (H69) 2000:1; (PC-7) 3500:1. (B) (PC-9) gefitinib: SN-38 = 6:1; (PC-9ZD) 175:1. Treatment schedule: (1) SN-38 was applied first and gefitinib was applied 12 h later, followed by incubation in medium for 72 h (blue). (2) SN-8 and gefitinib were applied concurrently, followed by incubation in medium for 72 h (red). (3) Gefitinib was applied first and SN-38 was applied 12 h later, followed by incubation in medium for 72 h (green). S → G: sequential combination (SN-38 followed by gefitinib); C/G: concurrent combination; G → S: sequential combination (gefitinib followed by SN-38).

cells were stained with anti-Ki-67, anti-CD31 and the TUNEL assay (Fig. 3A and B). A reduction in tumor cell proliferation (Ki-67 staining), a reduction in tumor vasculature (CD31 staining), and an increase in tumor apoptosis (TUNEL staining) were observed in tumors treated with gefitinib alone or gefitinib and CPT-11. The administration of CPT-11 alone increased the number of Ki-67 positive tumor cells. In the PC-9 tumors, sequential treatment resulted in a 2.7-fold increase in tumor cell apoptosis and a 1.9-fold decrease in vessel staining, compared with the results obtained in tumors treated concurrently. The ratio of apoptosis:proliferation increased 1.7-fold in sequentially treated tumors compared with tumors treated with both drugs concurrently. Quantitative analysis of tumor cell proliferation and apoptosis showed a significant difference between the effects of the concurrent and sequential schedules ($P < 0.001$), but not between concurrent and gefitinib-alone ($P > 0.01$ for all comparisons, Fig. 3C). No significant difference in CD31-positive cells was observed between the control and gefitinib-alone treatments, suggesting that gefitinib exerts no remarkable anti-angiogenetic effects ($P > 0.01$, Fig. 3C). Similar findings were observed in PC-9/ZD tumors. These findings suggest that the antitumor activity of sequential treatment using gefitinib and CPT-11 is mediated by an increase in tumor cell apoptosis, compared with concurrent treatment.

4. Discussion

The EGFR-targeting drug gefitinib has been approved in many countries for the treatment of NSCLC patients who have previously received chemotherapy. Previous preclinical models have demonstrated the synergistic effects of gefitinib and platinums or taxanes [8,9]. However, no significant difference in survival was demonstrated in two randomized placebo-controlled phase II trials examining over 2000 previously untreated patients with NSCLC. In these trials, gefitinib was given in combination with paclitaxel and carboplatin or with gemcitabine and cisplatin [10,11]. Different administration schedules for gefitinib and cytotoxic agents may be necessary for select populations.

EGFR gene mutations have been demonstrated in NSCLC, and patients with lung cancers expressing mutant EGFR are strongly suspected to be hypersensitive to gefitinib alone. An in-frame short deletion in exon 19 of EGFR is strongly related to hyperresponsiveness to gefitinib and other tyrosine kinase inhibitors [12,13]. Cells expressing this deletional EGFR mutation are hypersenstivie to EGFR-targeted tyrosine kinase inhibitors [5]. On the other hand, the treat-

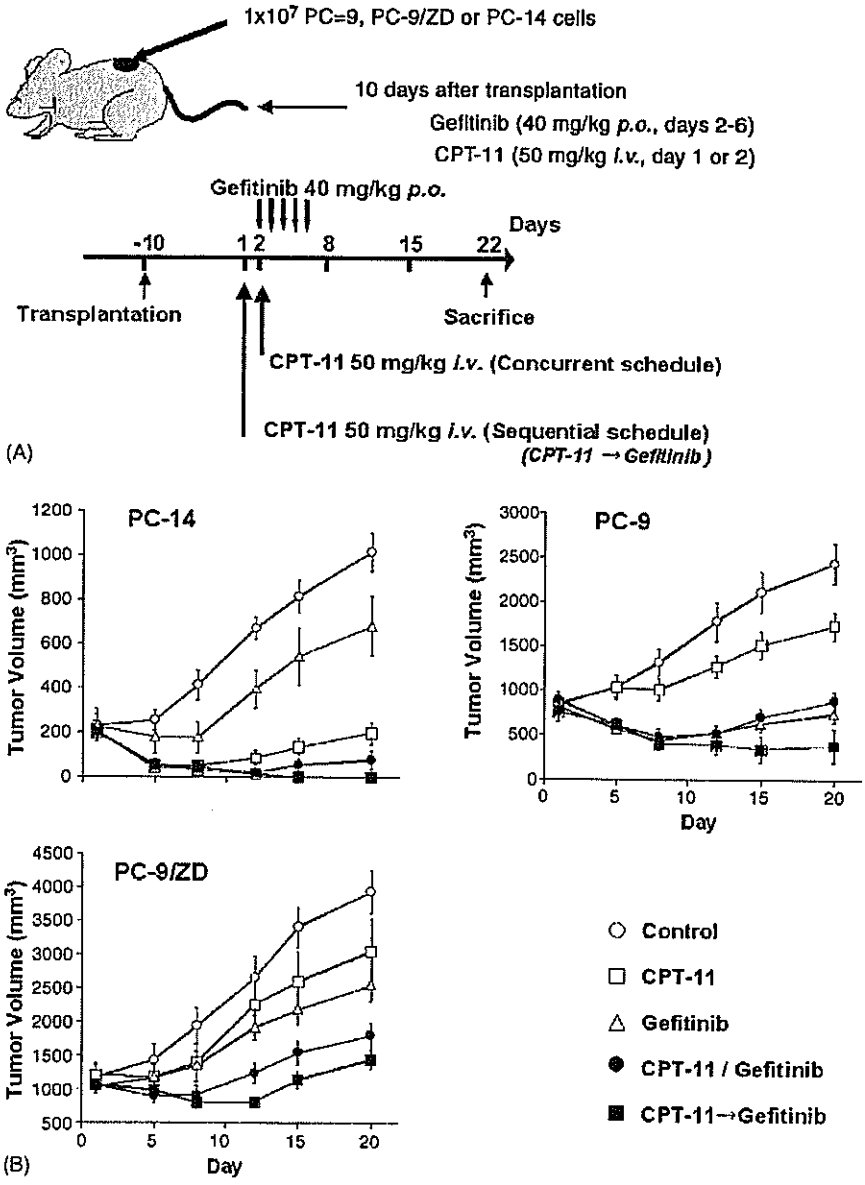

Fig. 2 Dose-dependent effects of combination therapy in PC9 and PC9/ZD cells in vivo. (A) Treatment schedule; (B) significant tumor growth-inhibition was observed in mice treated with the combination of gefitinib and CPT-11. Mice were allocated to five groups (6 mice/group) (○: 5% (w/v) glucose solution; □: CPT-11 50 mg/kg; △: gefitinib 40 mg/kg; ■: ZD1839 40 mg/kg + CPT-11 50 mg/kg concurrently; ●: CPT-11 50 mg/kg followed by ZD1839 40 mg/kg). (C) Treatment-related body weight loss in mice treated with gefitinib and/or SN-38. (○: 5% (w/v) glucose solution; □: CPT-11 50 mg/kg; △: ZD1839 40 mg/kg; ■: ZD1839 40 mg/kg + CPT-11 50 mg/kg concurrently; ●: CPT-11 50 mg/kg followed by ZD1839 40 mg/kg). Bars: ±S.D.

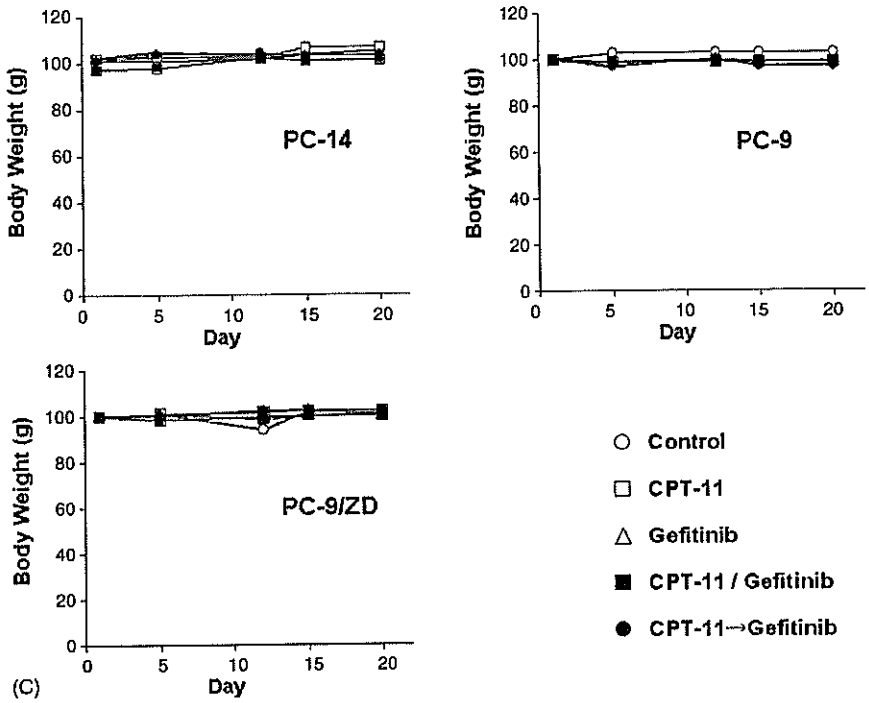

Fig. 2 (*Continued*).

ment of lung cancers expressing wild-type EGFR is a major obstacle. Combined therapies are still considered to be a major strategy against lung cancer expressing wild-type EGFR. Our previous preclinical study demonstrated that gefitinib and CPT-11 have synergistic effects in colorectal cancer cell lines [14]. Here, we reevaluated the combined effects of gefitinib and cytotoxic agents based on the status of EGFR mutations in lung cancer.

We demonstrated that gefitinib and SN-38, the active form of CPT-11, have synergistic or additive effects in lung cancer cells expressing wild-type EGFR. The combination of gefitinib and CPT-11 may be useful against lung cancers expressing wild-type EGFR. On the other hand, this combination had antagonistic effects in PC-9 cells expressing mutant EGFR, even though PC-9 cells are basically hypersensitive to gefitinib alone.

The concurrent administration of gefitinib and SN-38 also had an antagonistic effect in the PC-9/ZD cells. The PC-9/ZD cells developed an acquired resistance to gefitinib after exposure to gefitinib in vitro. New treatment strategies for patients who are refractory to gefitinib treatment are clinically needed. We demonstrated that the sequential administration of SN-38 (CPT-11) and gefitinib improved the combined effects in PC-9/ZD cells both in vitro and in vivo.

The above results led us to propose a combined gefitinib and CPT-11 treatment strategy based on the EGFR mutation status of lung cancers: (1) combined treatment according to any schedule for lung cancers expressing wild-type EGFR, (2) gefitinib treatment alone for lung cancers expressing mutant EGFR, and (3) the sequential administration of gefitinib and CPT-11 for patients who are refractory to gefitinib treatment. Based on the above preclinical evidence, we are preparing to begin a clinical phase II trial for combined gefitinib and CPT-11 treatment in Japan.

We previously demonstrated that CPT-11 and gefitinib have a synergistic effect against colorectal cancer [14]. EGFR mutations are rarely observed in colorectal cancer cells [15]. Therefore, the combined effects of these agents against colorectal cancers were consistent with those against the lung cancers expressing wild-type EGFR in this study.

Different combined effects were observed for the concurrent and sequential schedules in vitro and in vivo. While the mechanisms responsible for the combined effects remain unclear, cell cycle distributions might explain some of the differences. In cells treated according to the sequential gefitinib followed by SN-38 (CPT-11) treatment schedule, treatment with gefitinib resulted in an increase in the G0–G1 phase and a decrease in the S phase populations (data not shown). The decreased S phase population was not sensitive to CPT-11 [16]. Thus, the antagonistic effects of the sequential administration of gefitinib followed by CPT-11 (SN-38) could be explained by this mechanism. On the other hand, in cells treated according to the sequential SN-38 followed by gefitinib treatment schedule, SN-38 treatment induced an increase in the S phase population. If the S phase population is sensitive to gefitinib, this might explain the synergistic effects of this sequential schedule [17]. An increase in EGFR phosphorylation induced by CPT-11 is another previously reported possible mechanism responsible for this synergistic action [14].

In conclusion, we demonstrated the different effect on lung cancer cell expressing mutant EGFR according to the

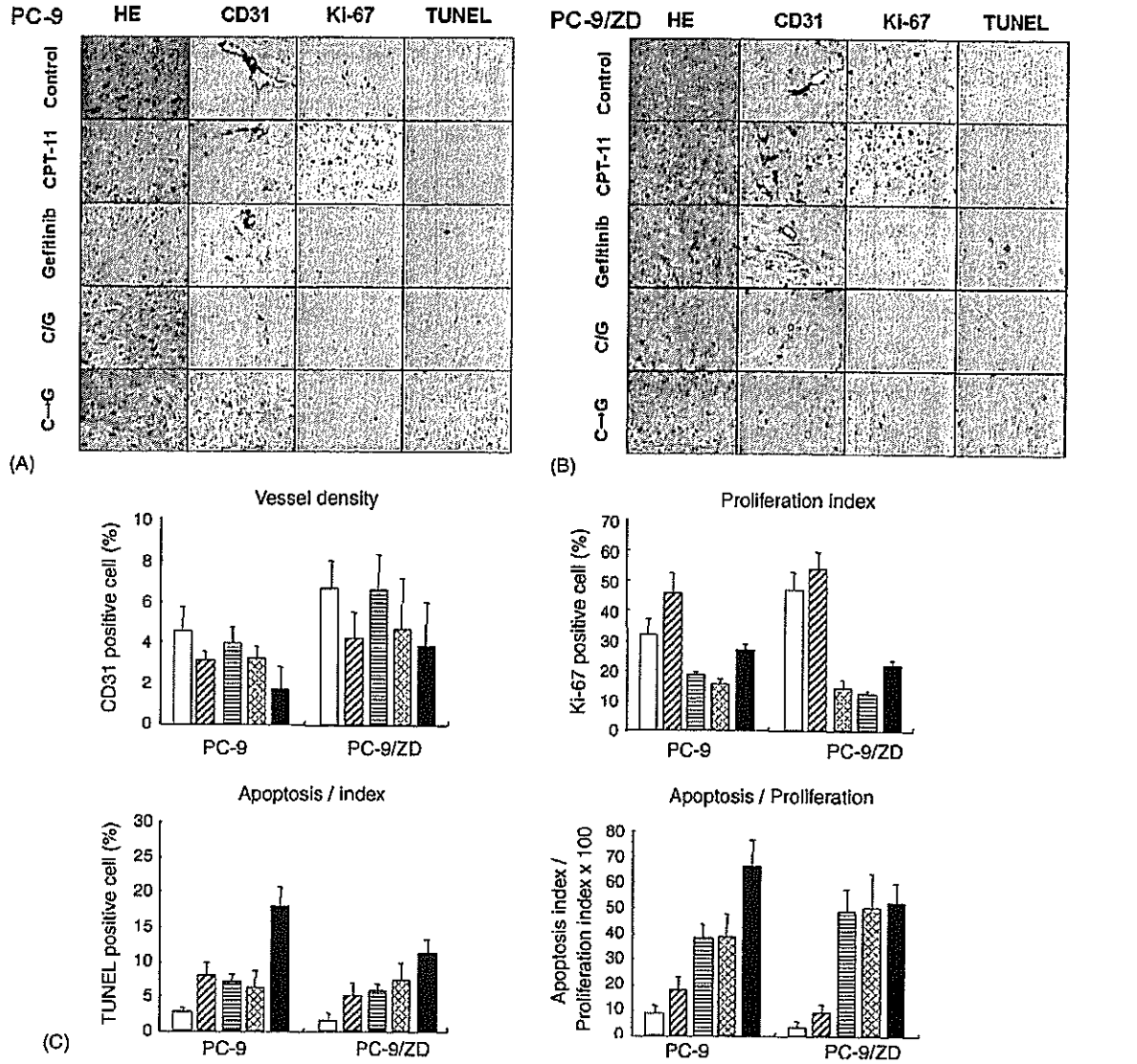

Fig. 3 (A) Historical examination of PC-9 tumor xenografts (day 22) stained with H&E, anti-CD31 vessel staining, TUNEL staining (magnification: 400×) and anti-Ki-67 nuclear antigen (magnification: 200×). The number of Ki-67-positive cells increased with the administration of CPT-11. The number of Ki-67-positive cells decreased with the gefitinib-alone and combination treatments. C/G: concurrent combination, C→ G: sequential combination. (B) Historical examination of PC-9ZD tumor xenografts (day 22) stained with H&E, anti-CD31 vessel staining, TUNEL staining (magnification: 400×) and anti-Ki-67 nuclear antigen (magnification: 200×). The number of Ki-67-positive cells increased with the administration of CPT-11. The number of Ki-67-positive cells decreased with the gefitinib-alone and combination treatments. C→ G: sequential combination; C/G: concurrent combination. (C) Quantitation of CD31 vessel staining, Ki-67 proliferation index, apoptosis index, and apoptosis: proliferation ratio. The columns represent the mean population of positive cells in five fields. Bars: ±S.D. Tumors from mice treated with vehicle (white), CPT-11 (diagonal hatched), Gefitinib (horizontal hatched), concurrent combination of CPT-11 plus Gefitinib (cross-hatched), or sequential combination of CPT-11 plus Gefitinib (cross-hatched).

combination schedule of gefitinib and CPT-11. The sequential combined treatment also active against lung cancer cell expressing wild-type EGFR.

Acknowledgements

This study was supported in part by a Grant-in-Aid for Cancer Research and the 3rd Term Comprehensive 10-Year Strategy for Cancer Control from the Ministry of Health, Labour and Welfare, Tokyo, Japan.

References

[1] Lynch TJ, Bell DW, Sordella R, Gurubhagavatula S, Okimoto RA, Brannigan BW, et al. Activating mutations in the epidermal growth factor receptor underlying responsiveness of non-small-

cell lung cancer to gefitinib. N Engl J Med 2004;350:2129–39.
[2] Paez JG, Janne PA, Lee JC, Tracy S, Greulich H, Gabriel S, et al. EGFR mutations in lung cancer: correlation with clinical response to gefitinib therapy. Science 2004;304:1497–500.
[3] Kobayashi S, Boggon TJ, Dayaram T, Janne PA, Kocher O, Meyerson M, et al. EGFR mutation and resistance of non-small-cell lung cancer to gefitinib. N Engl J Med 2005;352:786–92.
[4] Koizumi F, Shimoyama T, Taguchi F, Saijo N, Nishio K, Kanzawa F, et al. Establishment of a human non-small cell lung cancer cell line resistant to gefitinib Synergistic interaction between the EGFR tyrosine kinase inhibitor gefitinib ("Iressa") and the DNA topoisomerase I inhibitor CPT-11 (irinotecan) in human colorectal cancer cells. Int J Cancer 2005;116:36–44.
[5] Naruse I, Ohmori T, Ao Y, Fukumoto H, Kuroki T, Mori M, et al. Antitumor activity of the selective epidermal growth factor receptor-tyrosine kinase inhibitor (EGFR-TKI) Iressa (ZD1839) in an EGFR-expressing multidrug-resistant cell line in vitro and in vivo. Int J Cancer 2002;98:310–5.
[6] Kanzawa F, Akiyama Y, Saijo N, Nishio K. In vitro effects of combinations of cis-amminedichloro (2-methylpyridine) platinum(II) (ZD0473) with other novel anticancer drugs on the growth of SBC-3, a human small cell lung cancer cell line. Lung Cancer 2003;40:325–32.
[7] Chou TC, Talalay P. Quantitative analysis of dose-effect relationships: the combined effects of multiple drugs or enzyme inhibitors. Adv Enzyme Regul 1984;22:27–55.
[8] Ciardiello F, Caputo R, Bianco R, Damiano V, Pomatico G, De Placido S, et al. Antitumor effect and potentiation of cytotoxic drugs activity in human cancer cells by ZD-1839 (Iressa), an epidermal growth factor receptor-selective tyrosine kinase inhibitor. Clin Cancer Res 2000;6:2053–63.
[9] Sirotnak FM, Zakowski MF, Miller VA, Scher HI, Kris MG. Efficacy of cytotoxic agents against human tumor xenografts is markedly enhanced by coadministration of ZD1839 (Iressa), an inhibitor of EGFR tyrosine kinase. Clin Cancer Res 2000; 6:4885–92.
[10] Giaccone G, Herbst RS, Manegold C, Scagliotti G, Rosell R, Miller V, et al. Gefitinib in combination with gemcitabine and cisplatin in advanced non-small-cell lung cancer: a phase III trial—INTACT 1. J Clin Oncol 2004;22:777–84.
[11] Herbst RS, Giaccone G, Schiller JH, Natale RB, Miller V, Manegold C, et al. Gefitinib in combination with paclitaxel and carboplatin in advanced non-small-cell lung cancer: a phase III trial—INTACT 2. J Clin Oncol 2004;22:785–94.
[12] Taguchi F, Koh Y, Koizumi F, Tamura T, Saijo N, Nishio K. Anticancer effects of ZD6474, a VEGF receptor tyrosine kinase inhibitor, in gefitinib ("Iressa")-sensitive and resistant xenograft models. Cancer Sci 2004;95:984–9.
[13] Arao T, Fukumoto H, Takeda M, Tamura T, Saijo N, Nishio K. Small in-frame deletion in the epidermal growth factor receptor as a target for ZD6474. Cancer Res 2004;64:9101–4.
[14] Koizumi F, Kanzawa F, Ueda Y, Koh Y, Tsukiyama S, Taguchi F, et al. Synergistic interaction between the EGFR tyrosine kinase inhibitor gefitinib ("Iressa") and the DNA topoisomerase I inhibitor CPT-11 (irinotecan) in human colorectal cancer cells. Int J Cancer 2004;108:464–72.
[15] Barber TD, Vogelstein B, Kinzler KW, Velculescu VE. Somatic mutations of EGFR in colorectal cancers and glioblastomas. N Engl J Med 2004;351:2883.
[16] van Ark-Otte J, Kedde MA, van der Vijgh WJ, Dingemans AM, Jansen WJ, Pinedo HM, et al. Determinants of CPT-11 and SN-38 activities in human lung cancer cells. Br J Cancer 1998;77:2171–6.
[17] Park JK, Lee SH, Kang JH, Nishio K, Saijo N, Kuh HJ. Synergistic interaction between gefitinib (Iressa ZD1839) and paclitaxel against human gastric carcinoma cells. Anticancer Drugs 2004;15:809–18.

The Pharmacogenomics Journal (2006) 6, 388–396

www.nature.com/tpj

ORIGINAL ARTICLE

Reference profiling of the genomic response induced by an antimicrotubule agent, TZT-1027 (Soblidotin), *in vitro*

T Shimoyama[1,2], T Hamano[1], T Natsume[1], F Koizumi[1], K Kiura[2], M Tanimoto[2] and K Nishio[1,3]

[1]*Shien-Lab and Medical Oncology, National Cancer Center Hospital, Chuo-ku, Tokyo, Japan;* [2]*Department of Medicine II, Okayama University Medical School, Shikata-cho, Okayama, Japan and* [3]*Pharmacology Division, National Cancer Center Research Institution, Chuo-ku, Tokyo, Japan*

Correspondence:
Dr K Nishio, Shien-Lab, National Cancer Center Hospital, 5-1-1 Tsukiji, Chuo-ku, Tokyo 104-0045, Japan.
E-mail: knishio@gan2.res.ncc.go.jp

Received 24 October 2005; revised 20 January 2006; accepted 16 February 2006; published online 21 March 2006

TZT-1027 is an antimicrotubule agent targeting beta-tubulin that is undergoing clinical development. The genomic response of cancer cells to TZT-1027 was profiled to evaluate its biochemical activity. A lung cancer cell line, PC-14, was exposed to antimicrotubule agents including dolastatins, *Vinca* alkaloids and taxanes at an equivalent toxicity level. Alterations in the TZT-1027-induced gene expression of ~600 genes were then examined using microarray technology and the resulting gene profiles were compared with those for cells exposed to the other antimicrotubule agents. A principle component analysis using the whole gene set demonstrated that TZT-1027 produced similar gene profiles to those produced by dolastatin 10, but that these gene profiles differed from those produced by other agents. The agents were classified according to their induced genomic response in a molecular structure-dependent manner. Genes whose expression profiles differed according to drug class included intermediate filaments, extracellular matrix protein and Rho regulatory genes that may be involved in cytoskeletal and angiogenesis processes that are regulated by microtubule dynamics. TZT-1027 produces a unique genomic response profile distinct from that of *Vinca* alkaloids and taxanes, suggesting that this agent has a different mechanism of action. The selected genes may act as pharmacodynamic biomarkers allowing the unique mode of action of TZT-1027 to be discriminated from those of other antimicrotubule agents.
The Pharmacogenomics Journal (2006) **6**, 388–396. doi:10.1038/sj.tpj.6500386; published online 21 March 2006

Keywords: TZT-1027; dolastatin 10; cDNA microarray; taxanes; *Vinca* alkaloids; antimicrotubule agent

Introduction

Dolastatin 10 (D10) is small peptide inhibiting microtubule assembly and tubulin polymerization that was isolated in 1987 from an Indian Ocean mollusc, the sea hare (*Dolabella auricularia*).[1] Although D10 displayed significant antitumor activity in preclinical models and demonstrated good tolerability in clinical settings, recent phase II clinical trials suggested that D10, as a single agent, lacked significant activity.[2–5] TZT-1027 is a synthesized derivative of D10 with superior preclinical activity.[6] TZT-1027 showed notable antitumor activity against a broad range of human malignancies *in vivo*, including those resistant to conventional chemotherapeutic agents.[7] Superior antivascular activity resulting in the collapse

of the tumor vasculature was demonstrated, compared with the activities of taxanes and *Vinca* alkaloids.[8–10] The first clinical phase I study of TZT-1027 was initiated in 1994, and another four studies have since been completed; a phase II study is currently ongoing.[11–13] The major toxicity was hematological, in the form of neutropenia and leukopenia. Reversible peripheral neurotoxic syndrome, alopecia, fatigue and anorexia were the principal nonhematological toxicities.

TZT-1027 is a mitotic spindle poison that interacts with tubulin at the *Vinca* alkaloids binding site,[14] but the spectra of antitumor activity of TZT-1027 and the *Vinca* alkaloids are different *in vivo*.[7,10,15] TZT-1027 also showed potent antitumor activity against a vincristine-resistant cell line.[7] A recent investigation of the mode of action reported that TZT-1027-induced apoptosis and cell arrest in the G_2/M phase that was independent of caspase-3 or bcl-2.[16] According to *in vitro* studies performed with tumor tissue obtained from patients with lung and renal cell cancers, the activity of TZT-1027 is influenced less by the p53 mutation status than by DNA-damaging agents.[17] Despite these investigations, the mode of action and therapeutic class of TZT-1027 as an antimicrotubule agent remains unclear. To characterize the mode of action of this compound, microarray-based transcriptional profiles have been performed.[18,19]

Cell-based high-throughput screening technologies provide information about cellular pathways that control drug sensitivity.[20,21] Drug-to-drug comparative approaches using microarray analyses are useful for identifying drug targets; the cellular effects caused by a novel drug of incompletely characterized specificity can be matched to 'reference profiles' of the cellular effects elicited by the specific inhibition of candidate analog-sensitive drugs.[22,23] Thus, it has been proposed that phenotypic information generated by drug-induced alterations in gene expression can be matched to discrete interactions between the compound and the relevant protein targets. Using the drug-to-drug comparative approach of the microarray analysis, we obtained reference profiles of genomic expression data from cellular responses in a lung cancer cell line to antimicrotubule drugs, including five conventional agents and the mother compound D10. In the present study, we aimed to characterize TZT-1027 using these reference profiles.

Results

Growth inhibition

The growth inhibitory effect of TZT-1027 and the other six antimicrotubule agents was determined using an MTT assay. The PC-14 cell line was exposed to each drug for 72 h. The 50% growth inhibitory concentrations (IC_{50} values) were as follows: TZT-1027, 0.02 nM; D10, 0.1 nM; VDS, 4 nM; VBL, 2 nM; VCR, 7 nM; TXL, 3 nM and TXT, 3 nM. Based on these results, TZT-1027 was over a hundred times more cytotoxic than the other taxanes and *Vinca* alkaloids.

Microarray data mining

The expression intensity of the array was normalized using a global normalization method. The change in gene expression was calculated as the intensity ratio between treated and untreated samples. The complete cDNA microarray data can be found in the Supplementary Tables. This supporting information contains the raw data, normalized data and a summary of the selected genes.

Common genes regulated by all antimicrotubule agents

Of the 588 genes that were surveyed in the microarray analysis, 118 genes were upregulated by all seven antimicrotubules

Table 1 Gene ontology analysis of biological process of antimicrotubule agents

Upregulated		*Downregulated*	
Gene category	P	*Gene category*	P
G2/M transition of mitotic cell cycle	<0.0001	Cell–cell signaling	<0.0001
Cytokinesis	<0.0001	Morphogenesis	<0.0001
Regulation of cell cycle	0.0002	Organogenesis	0.0001
Obsolete biological process	0.0003	Development	0.0001
G1/S transition of mitotic cell cycle	0.0004	Cell communication	0.0001
Mitotic cell cycle	0.0008	Positive regulation of cell proliferation	0.0042
Apoptosis	0.0009	Growth	0.0074
Cell cycle	0.0010	Immune response	0.0098
Programmed cell death	0.0012	Defense response	0.0098
Cell death	0.0012		
Death	0.0012		
Regulation of CDK activity	0.0012		
Positive regulation of programmed cell death	0.0077		
Positive regulation of apoptosis	0.0077		
Induction of apoptosis	0.0077		
Regulation of programmed cell death	0.0077		
Induction of programmed cell death	0.0077		

agents. A functional analysis of these genes was performed using EASE, and the results are listed in Table 1. The results showed that genes associated with cell-cycle regulation, mitosis or apoptosis were significantly upregulated by the antimicrotubules agents. Among the downregulated genes, 141 genes that were associated with cell communication and morphogenesis were selected. These results suggested that transcription regulation by antimicrotubule agents results in the biological inhibition of microtubule dynamics.

Drug characterization using molecular reference profiles

Focusing on the 'reference profiles' of the drug-induced genomic response, we compared the profiles of TZT-1027 with those of five conventional antimicrotubule agents and the mother compound, D10.

A principle component representation of the whole gene set in three-dimensional space clearly showed the relationship between TZT-1027 and the other six reference profiles (Figure 1). All the drugs were separated according to each drug class in this profile. In comparison with these reference profiles, TZT-1027's profile was similar to that of D10 but different from those of the taxanes and *Vinca* alkaloids.

To investigate the differences in genomic response between the drug classes, we selected discriminatory genes that were regulated differently between the drug classes, compared with the complete gene set. Table 2 shows the genes whose expression profiles differed after exposure to dolastatins (TZT-1027 and D10) and the other antimicrotubule agents. The most discriminatory gene in this gene set was the drug-resistant gene, *GSTO1*. Using this gene set, the classes of antimicrotubule agents could be clearly separated (Figure 2a). Discriminatory gene sets for the taxanes and *Vinca* alkaloids were obtained in a similar manner (Tables 3 and 4). The profiles of the discriminatory gene sets for the taxanes and *Vinca* alkaloids are shown in Figure 2b and c.

To further characterize TZT-1027, the genes that were regulated differently after exposure to TZT-1027 and D10 were investigated. Six genes that were regulated differently by a factor of more than one in a log ratio after exposure to each agent were selected (Table 5). Four cytoskeletal genes were included in this group. A three-dimensional representation using these six genes demonstrated that the profiles

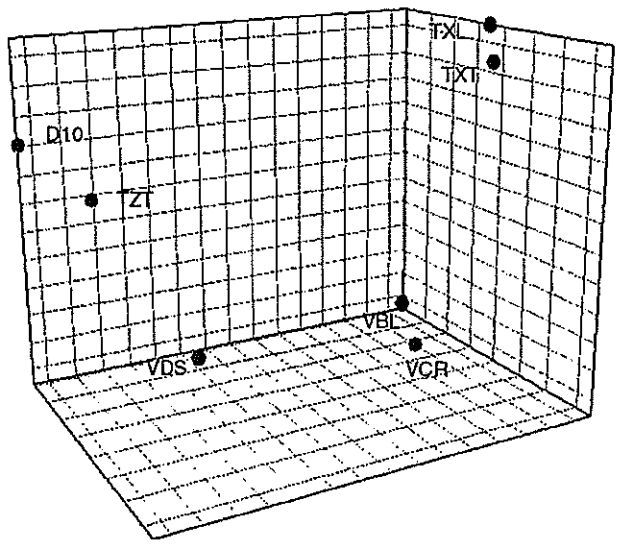

Figure 1 Three-dimensional representation of antimicrotubule agents according to a principle component analysis of the gene expression data for 588 genes. In this analysis, samples with similar expression profiles lie closer to each other than those with dissimilar profiles. The graph shows a robust class separation into three major categories: dolastatins, *Vinca* alkaloids and taxanes. TZT, TZT-1027; dolastatin 10, D10; VDS, vindesine; VCR, vincristine; VBL, vinblastine; TXL, paclitaxel; TXT, docetaxel.

Table 2 Discriminatory genes of dolastatins (D 10 and TZT-1027)

GB	*Symbol*	*Description*	*Log ratio*			
			D10	*TZT*	*VA*	*TX*
Upregulated genes						
U90313	GSTO1	Glutathione-*S*-transferase homolog	0.905	0.189	−0.818	−0.706
Z30183	TIMP3	Tissue inhibitor of metalloproteinase 3	0.703	0.481	−0.343	−0.859
U46461	DVL	Disheveled, dsh homolog 1	0.206	0.396	−0.542	−0.444
J00124	KRT1	50 kDa type I epidermal keratin	0.190	0.278	−0.643	−0.219
M57765	IL11	Interleukin 11	0.124	0.454	−0.342	−0.493
M74088	APC	Adenomatosis polyposis coli	0.040	0.069	−0.224	−0.582
Downregulated genes						
U02570	RhoGAP1	Rho-related small GTPase protein activator	−0.048	−0.076	0.433	0.248
J04177	COL11A1	Collagen, type XI, alpha 1	−0.048	−0.290	0.388	0.074
X72925	DSC1	Desmocollin-1	−0.117	−0.051	0.346	0.388
U35835	DNA-PK	DNA-dependent protein kinase	−0.215	−0.241	0.596	0.648
M65290	IL12B	Interleukin 12 beta	−0.322	−0.134	0.351	1.070

Abbreviations: GB, genebank accession number; D10, dolastatin 10; TZT, TZT-1027; VA, average of *Vinca* alkaloids including vincristine, vindesine, vinblastine; TX, average of taxanes including paclitaxel and docetaxel.

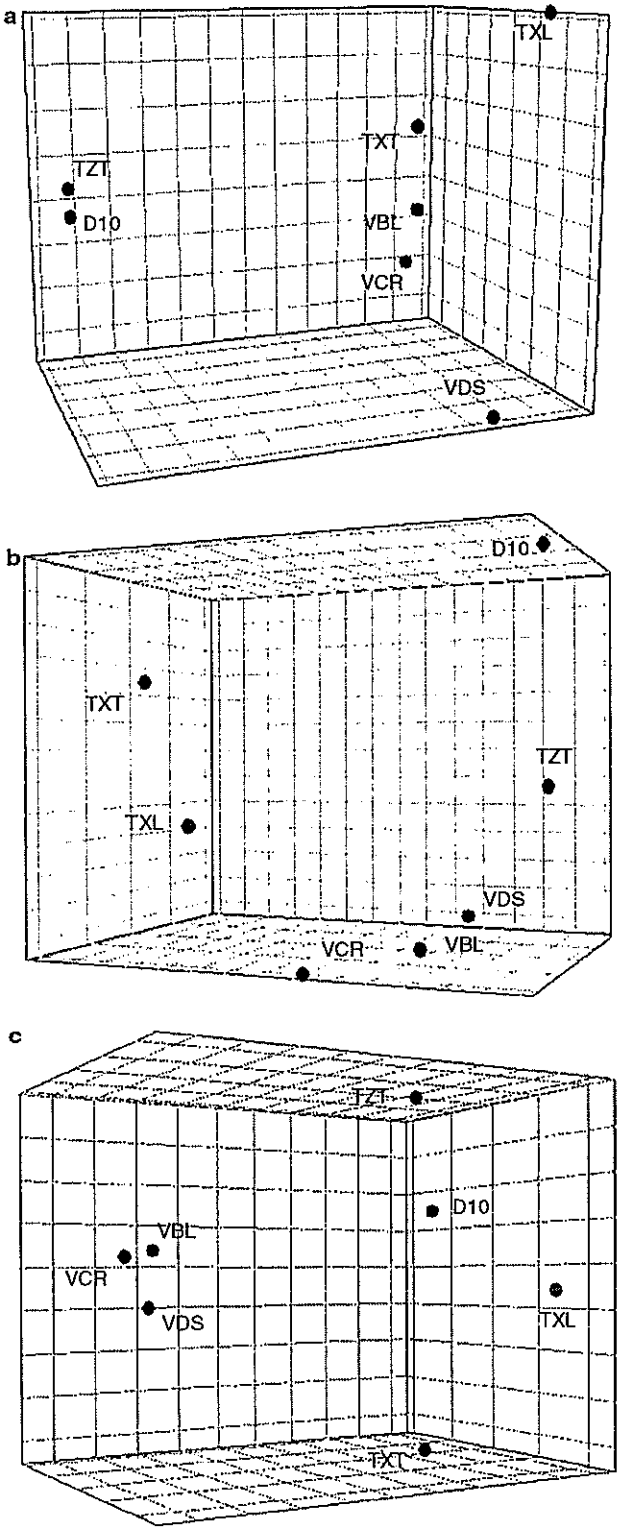

of the taxanes and *Vinca* alkaloids differed from those of TZT-1027 and D10 (Figure 3).

Validation of discriminatory genes by RT-PCR

The identified discriminatory genes GSTO1 and TIMP3 were validated using real-time RT-PCR (Figure 4). To investigate whether the genomic responses of these genes depended on the cytotoxicity levels, the RT-PCR experiment was performed at different cytotoxicity levels (IC_{90} and IC_{10}) of TZT-1027. The results are summarized in Figure 5. These findings suggested that the selected genomic responses might not depend on the cytotoxicity levels, whereas the genomic response of GSTO1 demonstrated a dose dependency.

Discussion

In the present study, we characterized the novel antimicrotubule agent TZT-1027 using a microarray analysis. Dolastatins belong to a class of microtubule-destabilizing agents, but this classification is not sufficient for clinical use. Despite similarities in their mechanism of action and structure, antimicrotubule agents differ in their antitumor and toxicologic profiles.[24] It now seems that the most important action of antimicrotubule agents is not the regulation of microtubule-polymer mass (polymerization and depolymerization), but the suppression of spindle-microtubule dynamics.[25] Furthermore, many of the drugs act not only on microtubules, but also on soluble tubulin, and the location of the specific binding site in tubulin and microtubules greatly affects the response of the microtubule system to the drug.[25] Therefore, to characterize the novel antimicrotubule agent TZT-1027, we analyzed drug-induced changes in gene expression using the microarray technique and compared the molecular profiles with those induced by the mother compound, D10, and other well-known antimicrotubule agents, such as *Vinca* alkaloids and taxanes.

For the profiles, we evaluated the IC_{50} value of each drug using a growth inhibitory assay. We aimed to categorize the drugs based on their mechanisms of action; therefore, the changes in gene expression were, of necessity, induced at the same cytotoxicity level. The resulting expression profiles were obtained using a microarray containing ~600 key genes applicable to antimicrotubule drug research, including genes involved with microtubule dynamics, cell-cycle regulation, angiogenesis and the extracellular matrix as well as cell adhesion receptors, oncogenes and tumor-suppressor genes. We focused on changes in gene expression because gene regulation should be correlated with the protein status modulated by the drugs.

Figure 2 Spatial class separation of antimicrotubule agents using specific discriminatory genes. The axes represent the first three linear discriminants of the expression levels of (**a**) 11 dolastatin-discriminatory genes from Table 2, (**b**) 9 taxane-discriminatory genes from Table 3 and (**c**) 5 *Vinca* alkaloid-discriminatory genes from Table 4. TZT, TZT-1027; dolastatin 10, D10; VDS, vindesine; VCR, vincristine; VBL, vinblastine; TXL, paclitaxel; TXT, docetaxel.

Table 3 Discriminatory genes of taxanes (paclitaxel, docetaxel)

GB	Symbol	Description	Log ratio			
			TX	VA	D10	TZT
Upregulated genes						
X02492	G1P3	Interferon-induced protein 6–16 precursor	1.122	−0.397	−1.150	−0.902
Y10256	NIK	Serine/threonine protein kinase	0.637	−0.951	−0.595	−0.287
U72661	NINJ1	Ninjurin 1	0.481	−0.154	−1.015	−0.448
M65199	ET2	Endothelin 2	0.444	−0.488	−2.185	−1.507
X54936	PlGF	Placenta growth factor	0.345	−0.235	−0.677	−0.602
X01992	IFN-gamma	Interferon, gamma	0.251	−0.929	−1.005	−1.583
Downregulated genes						
AF010309	PIG3	Tumor protein p53 inducible protein 3	−0.036	0.366	0.957	0.652
M76125	UFO	Tyrosine-protein kinase receptor UFO precursor	−0.132	0.201	0.020	0.329
U39657	MKK6	Mitogen-activated protein kinase 6	−0.204	0.554	0.740	0.368

Abbreviations: GB, genebank accession number; TX, average of taxanes including paclitaxel and docetaxel; VA, average of *Vinca* alkaloids including vincristine, vindesine, vinblastine; D10, dolastatin 10; TZT, TZT-1027.

Table 4 Discriminatory genes of *Vinca* alkaloids (vindesine, vincristine, vinblastine)

GB	Symbol	Description	Log ratio			
			VA	TX	D10	TZT
Upregulated genes						
X14787	TSP1	Thrombospondin 1	0.319	−0.230	−0.106	−0.019
X07820	MMP10	Matrix metalloproteinase 10	0.273	−0.272	−0.297	−0.417
Downregulated genes						
D78367	KRT12	Keratin 12	−0.124	0.262	0.250	0.598
X03212	KRT7	Keratin 7	−0.168	0.412	0.004	0.290
X56134	VIM	Vimentin	−1.072	0.583	0.927	1.344

Abbreviations: GB, genebank accession number; VA, average of *Vinca* alkaloids including vincristine, vindesine, vinblastine; TX, average of taxanes including paclitaxel and docetaxel; D10, dolastatin 10; TZT, TZT-1027.

Table 5 Discriminatory genes between TZT-1027 and dolastatin 10

GB	Symbol	Description	Log ratio						
			TZT	D10	VDS	VBL	VCR	TXL	TXT
U59167	DESM	Desmin	1.74	−0.49	−0.28	0.06	−0.71	0.44	0.43
U34819	MAPK10	Mitogen-activated protein kinase 10	0.83	−0.69	−0.52	0.98	0.57	1.33	0.93
X14420	COL3A1	Collagen, type III, alpha 1	0.52	−0.92	0.56	−0.79	−0.38	−0.67	−0.66
X05610	COL4A2	Collagen, type IV, alpha 2	0.71	−0.53	0.82	0.32	0.10	−0.06	0.33
X16468	COL2A1	Collagen, type II, alpha 1	1.08	−0.01	0.99	−0.08	0.56	0.36	−0.07
U33635	PTK7	Tyrosine-protein kinase-like 7	0.62	−0.45	0.04	0.56	0.68	0.15	0.05

Abbreviations: GB, genebank accession number; TZT, TZT-1027; D10, dolastatin 10; VDS, vindesine; VBL, vinblastine; VCR, vincristine; TXL, paclitaxel; TXT, docetaxel.

Of the 588 genes that were surveyed, about half of all the genes were regulated similarly by the seven drugs. The probability of these similar expression profiles occurring by chance is almost zero ($P<1\times10^{-100}$). Furthermore, the functions of the clustered genes were associated with microtubule dynamics. The 118 genes that were upregulated were significantly associated with cell-cycle regulation, mitosis or apoptosis, whereas the 141 genes that were

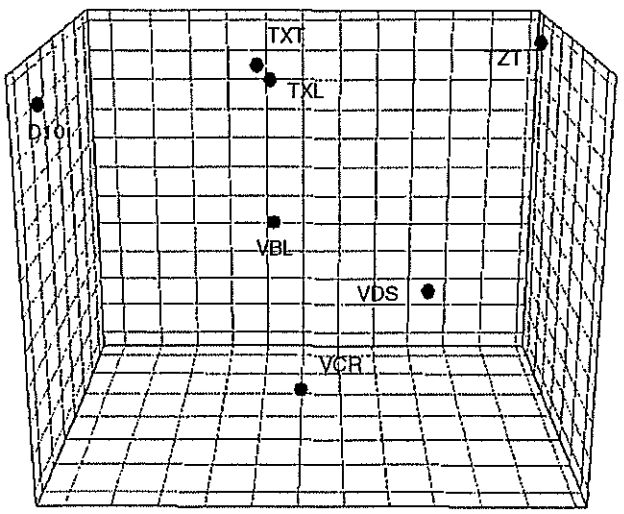

Figure 3 Spatial class separation of antimicrotubule agents using six genes from Table 5 that discriminated between TZT-1027 and dolastatin 10. TZT and D10 were distant from all the other antimicrotubule agents. TZT, TZT-1027; dolastatin 10, D10; VDS, vindesine; VCR, vincristine; VBL, vinblastine; TXL, paclitaxel; TXT, docetaxel.

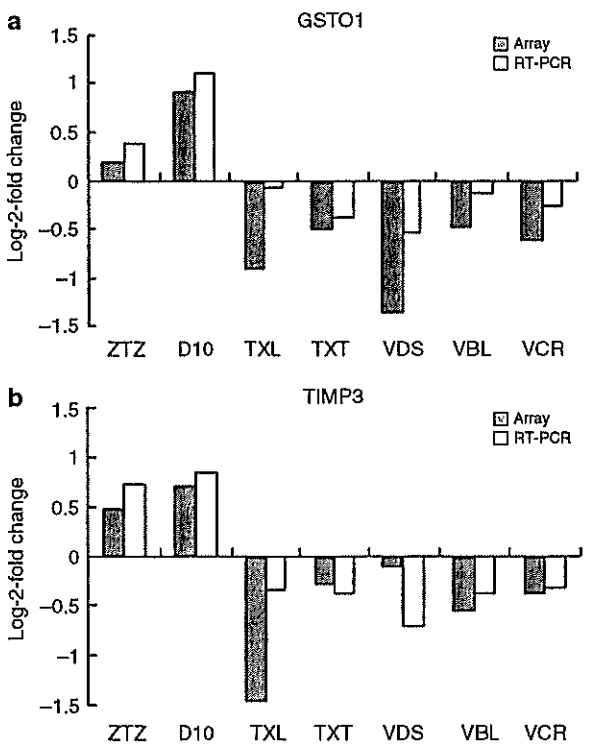

Figure 4 Gene expression of GSTO1 and TIMP3 in PC-14 cells treated with antimicrotubule agents. Validation of mRNA expression levels in PC-14 cells after 6 h of treatment with TZT-1027 (TZT), dolastatin 10 (D10), paclitaxel (TXL), docetaxel (TXT), vindesine (VDS), vinblastine (VBL) or vincristine (VCR). Relative mRNA amounts were normalized with respect to expression levels in untreated PC-14 cells (Log-2-fold change = 0).

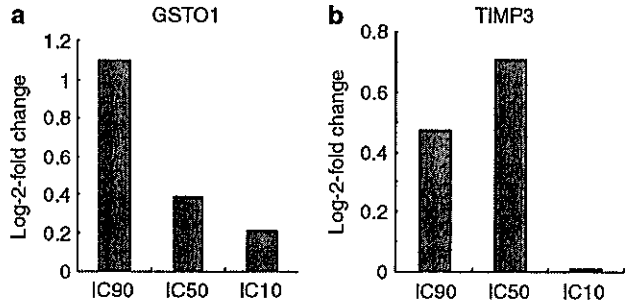

Figure 5 (a) Gene expression of GSTO1 in PC-14 cells treated with TZT-1027 at IC_{90}, IC_{50} or IC_{10}. (b) Gene expression of TIMP3 in PC-14 cells treated with TZT-1027 at IC_{90}, IC_{50} or IC_{10}. Validation of mRNA expression levels in PC-14 cells after 6 h of treatment with TZT-1027 (TZT) at IC_{90} (0.1 nM) or IC_{10} (0.005 nM).

downregulated were associated with cell communication and morphogenesis. Therefore, we concluded that the genomic response profiles represented the drug activities in PC-14 cells and investigated the discriminatory genes within each drug class to enable their further characterization.

By comparing the resulting gene profiles, each drug was categorized according to its drug class based on its effects on microtubule modulation (Figure 1). This finding suggested that genomic response was mostly affected by the drug-binding site on the microtubules. TXT shares the same tubulin-binding site as TXL, and this site is distinct from the *Vinca* alkaloids binding site.[25] Although TXL has a 1.9-fold higher affinity for the binding site and polymerizes tubulin at 2.1-fold lower concentrations than TXL,[26] TXL and TXT induced similar gene expression profiles, compared with those induced by the other antimicrotubule drugs. Among the three *Vinca* alkaloids (VBL, VDS and VCR), the expression profile of VDS differed from those of the other two (Figure 6). Natsume *et al.*[14] reported that all three *Vinca* alkaloids inhibited the polymerization of microtubules at a similar affinity. VBL and VCR are structurally very similar, whereas the structure of VDS differs from those of the other two.[27] This structural difference may be responsible for the different genomic responses. *Vinca* alkaloids and dolastatins are known to bind at so-called *Vinca*-binding domains in tubulin.[25] They share the same binding site and have similar affinities,[14,28] whereas additional binding sites have either high affinities (Kd: 1–2 μmol) or low affinities (Kd: 0.25–3 μmol).[24] Previous studies have also reported that dolastatins can also bind at different sites from those used by *Vinca* alkaloids[14,29] These additional binding sites might be responsible for the differences in genomic response induced by the dolastatins and *Vinca* alkaloids.

Interestingly, of the 31 discriminatory genes that were selected, six of them were intermediate filament (IF) genes like desmin, vimentin, desmocollin and keratin (Tables 2, 4, 5). In addition, four collagen genes and one Rho-regulator gene were also selected. These genes are all associated with cytoskeletal regulation by the Rho signaling pathway via

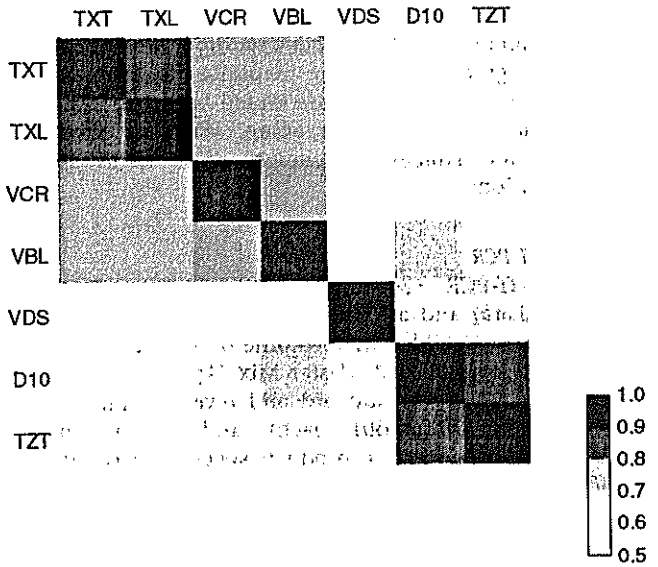

Figure 6 Heat map of correlations between drug profiles. Gene expression profiles containing data for 588 genes were compared after exposure to each drug to derive a matrix of Pearson correlation coefficients indicating the degree of overall similarity between any two drugs. A high-positive correlation is shown in red, and a low-positive correlation is shown in white. In this graph, TZT and D10 had the most similar expression profiles. TZT, TZT-1027; dolastatin 10, D10; VDS, vindesine; VCR, vincristine; VBL, vinblastine; TXL, paclitaxel; TXT, docetaxel.

microtubule dynamics.[30] Rho proteins also modulate the extracellular matrix either by regulating the levels of MMPs (matrix metalloproteinase) or their antagonists, TIMPs (tissue inhibitor of metalloproteinase).[31] These results suggested that the difference in the tubulin-drug binding site might regulate the difference in the signal transduction.

Of the genes that discriminated between dolastatins and the other drug class, the most significant genes were GSTO1 and TIMP3. GSTO1 (glutathione transferase omega 1) is a member of the glutathione *S*-transferase (GST) family of phase II enzymes that catalyze glutathione-dependent detoxification.[32] The role of GST has been evaluated in drug resistance. Schisselbauer *et al.* [33]reported that an elevated GST level in tumors was detected after the development of clinical drug resistance. Ban *et al.*[34] reported that adriamycin, cisplatin and etoposide increased tumor sensitivity by inhibiting GST expression in a colon cancer cell line, but TXL and VCR did not alter sensitivity. TIMP3 is a protein that binds to the extracellular matrix[35] and belongs to a family of endogenous MMP inhibitors. Members of the MMP family play important roles in angiogenesis.[36] Therefore, TIMP3 is regarded as a potent inhibitor of angiogenesis and tumor growth.[37] Qi *et al.*[38] reported that TIMP3 blocks the binding of VEGF (vascular endothelial growth factor) to the VEGF receptor-2, inhibiting downstream signaling and angiogenesis. TZT-1027 showed antitumor activity *in vivo* against a hypervascular advanced-stage tumor from a VEGF-transfectant lung cancer cell line, whereas VCR and TXT did not.[10] The upregulation of TIMP3 by TZT-1027 is one possible mechanism for the superior antivascular activity of this drug, compared to that of taxanes and *Vinca* alkaloids.

To analyze whether similar genomic responses occurred in lung cancer cell lines other than PC-14, RT-PCR for GSTO1 and TIMP3 was performed in another lung cancer cell line, SBC-3, treated with TZT-1027 at IC_{50}. GSTO1 and TIMP3 were downregulated in SBC-3 cells treated with dolastatins and upregulated in the cells treated with the other antimicrotubule agents, opposite to the profile seen for PC-14 cells (data not shown). This result suggested that these genes may have different genomic responses in other lung cancer cells.

This was a 'proof-of-principle study'. We demonstrated the various cellular responses to antimicrotubule agents at a gene expression level, even though the agents targeted the same molecules. We believe that this approach to characterizing drugs *in vitro* may be useful in clinical settings in that surrogate tissue, like peripheral blood mononuclear cells, can be used. The present findings obtained using our microarray analysis could greatly help us to understand the mode of action of TZT-1027 and other antimicrotubule agents. This capacity to identify therapeutic efficacy on the basis of gene expression signatures *in vitro* may be useful for drug discovery and drug target validation.

Materials and methods

Cell lines and cultures

A human non-small-cell-lung cancer cell line, PC-14, was provided by Professor Y Hayata, Tokyo Medical College. PC-14 was grown in RPMI-1640 medium (Nikken BioMedical Laboratory, Kyoto, Japan) supplemented with 10% fetal bovine serum, penicillin G and 100 μg/ml streptomycin solution and was maintained in a humidified 5% CO_2 atmosphere at 37°C.

Drugs and culture

TZT-1027 and D10 were provided by Teikoku Hormone Mfg. Co. Ltd (Kawasaki, Japan) and were dissolved in and diluted with 0.05 M lactate buffer (pH 4.5). Vindesine (VDS), vincristine (VCR), vinblastine (VBL), docetaxel (TXT) and paclitaxel (TXL) were obtained from Shionogi Co. (Osaka, Japan), Shionogi Pharmaceutical Co. (Osaka, Japan), Kyorin Pharmaceutical Co. Ltd (Tokyo, Japan), Chugai-Seiyaku Co, Ltd (Tokyo, Japan) and Bristol-Myers Japan (Tokyo, Japan), respectively. RPMI 1640 medium (Gibe-BRL) and fetal bovine serum were purchased from Nisus (Tokyo, Japan).

MTT assay

The inhibitory effect of the drugs on the PC-14 cell line was determined using a colorimetric assay (MTT assay) according to the method of Mosmann.[39]Briefly, 10^3 cells were harvested in 96-well microtiter plates (Becton Dickinson & Co.) in a volume of 180 μl and incubated for 24 h at 37°C in humidified air containing 5% CO_2. Each drug was added to